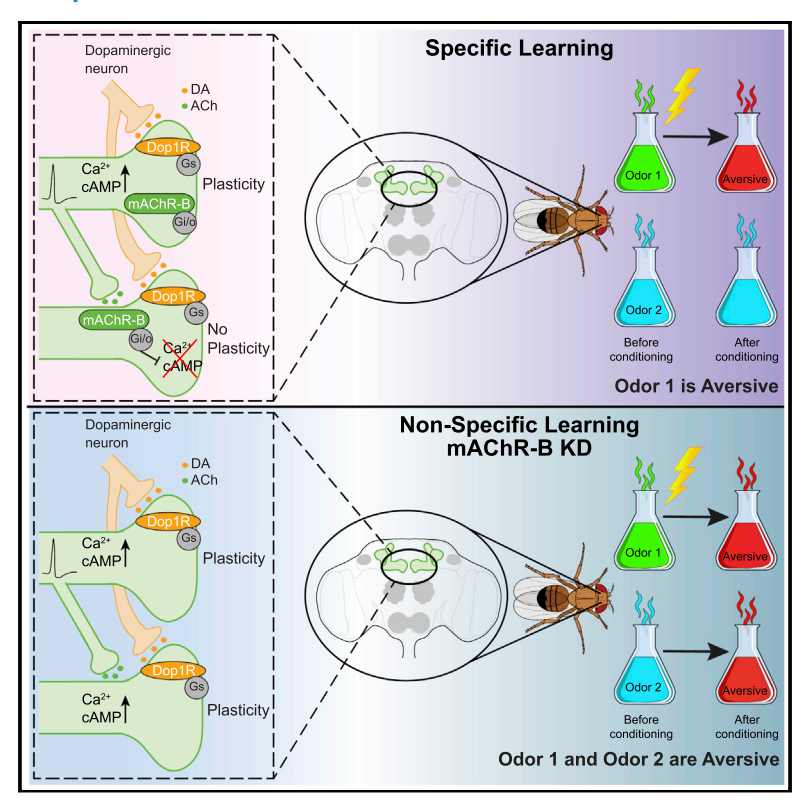
Lateral axonal modulation is required for stimulusspecific olfactory conditioning in *Drosophila*

Graphical abstract



Authors

Julia E. Manoim, Andrew M. Davidson, Shirley Weiss, Toshihide Hige, Moshe Parnas

Correspondence

hige@email.unc.edu (T.H.), mparnas@tauex.tau.ac.il (M.P.)

In brief

Manoim et al. show that the abundant axo-axonic synapses between Kenyon cells in *Drosophila* mushroom body are mediated by muscarinic type-B receptors, which suppress Ca²⁺ and cAMP signals in neighboring cells. Since both signals are essential for synaptic plasticity, the lateral suppression enhances the stimulus specificity of associative learning.

Highlights

- Lateral KC axo-axonic connections are mediated by muscarinic type-B receptor
- KC connections suppress odor-evoked calcium responses and dopamine-evoked cAMP
- Knockdown of the muscarinic type-B receptor impairs olfactory learning
- Impaired learning is due to changes to the valence of the unconditioned odor



Current Biology



Article

Lateral axonal modulation is required for stimulus-specific olfactory conditioning in *Drosophila*

Julia E. Manoim, ^{1,7} Andrew M. Davidson, ² Shirley Weiss, ¹ Toshihide Hige, ^{2,3,4,*} and Moshe Parnas ^{1,5,6,8,*}

- ¹Department of Physiology and Pharmacology, Sackler School of Medicine, Tel Aviv University, Tel Aviv 69978, Israel
- ²Department of Biology, University of North Carolina at Chapel Hill, Chapel Hill, NC 27599, USA
- 3Department of Cell Biology and Physiology, University of North Carolina at Chapel Hill, Chapel Hill, NC 27599, USA
- ⁴Integrative Program for Biological and Genome Sciences, University of North Carolina at Chapel Hill, Chapel Hill, NC 27599, USA
- ⁵Sagol School of Neuroscience, Tel Aviv University, Tel Aviv 69978, Israel
- ⁶Twitter: @MosheParnas ⁷Twitter: @JManoim
- ⁸Lead contact

*Correspondence: hige@email.unc.edu (T. H.), mparnas@tauex.tau.ac.il (M. P.)

https://doi.org/10.1016/j.cub.2022.09.007

SUMMARY

Effective and stimulus-specific learning is essential for animals' survival. Two major mechanisms are known to aid stimulus specificity of associative learning. One is accurate stimulus-specific representations in neurons. The second is a limited effective temporal window for the reinforcing signals to induce neuromodulation after sensory stimuli. However, these mechanisms are often imperfect in preventing unspecific associations; different sensory stimuli can be represented by overlapping populations of neurons, and more importantly, the reinforcing signals alone can induce neuromodulation even without coincident sensory-evoked neuronal activity. Here, we report a crucial neuromodulatory mechanism that counteracts both limitations and is thereby essential for stimulus specificity of learning. In Drosophila, olfactory signals are sparsely represented by cholinergic Kenyon cells (KCs), which receive dopaminergic reinforcing input. We find that KCs have numerous axo-axonic connections mediated by the muscarinic type-B receptor (mAChR-B). By using functional imaging and optogenetic approaches, we show that these axo-axonic connections suppress both odor-evoked calcium responses and dopamine-evoked cAMP signals in neighboring KCs. Strikingly, behavior experiments demonstrate that mAChR-B knockdown in KCs impairs olfactory learning by inducing undesired changes to the valence of an odor that was not associated with the reinforcer. Thus, this local neuromodulation acts in concert with sparse sensory representations and global dopaminergic modulation to achieve effective and accurate memory formation.

INTRODUCTION

An animal's survival critically depends on its capacity for sensory discrimination, which enables stimulus-specific modulation of behavior. In associative learning, a particular sensory input is associated with reward or punishment. Across animal phyla, dopamine (DA) plays a central role in mediating those reinforcement signals and inducing synaptic plasticity. The majority of DA signaling is mediated by volume transmission,² but this only provides coarse spatial specificity. Neuromodulation must be further restricted to the few synapses whose activity represents the specific sensory stimulus that is being associated with the reinforcer. One important contributing mechanism to such synapse specificity is the requirement of temporal coincidence of DA input and synaptic activity for plasticity. That is, plasticity only occurs at synapses that are co-active with (or were active immediately before) DA input.³⁻⁵ Another important mechanism observed in many cortical areas to help synapse

specificity is the sparse coding of sensory representations, 6-10 which minimizes overlap between neuronal subpopulations whose activity represents distinct stimuli. This combination of a short eligibility time window and segregated sensory representation is assumed to underlie stimulus specificity of learning. 11,12 However, it is known that as sensory signals ascend to higher brain areas, there is an inherent increase in trial-to-trial variability 13-15 that might risk the reliability of sparse representation as well as stimulus specificity of learning. In this study, we identified additional novel processes acting locally at axons to enhance synapse specificity of plasticity induction beyond that which can be accomplished at the neuronal population level.

In *Drosophila* olfactory learning, convergence of sensory and reinforcement signals takes place at axons of Kenyon cells (KCs), which are the third-order olfactory neurons constituting the principal neurons of the mushroom body (MB). ¹⁶ Specific DA neurons (DANs) densely innervate specific segments of the KC axon bundles. ^{17–19} The spatial arrangement of DAN-KC



synapses revealed in the EM connectome suggests that DA modulation occurs by volume, rather than local, transmission.²⁰ Thus, like in vertebrate brains, release of DA is unlikely to be target specific in the MB. Associative learning in flies almost completely depends on G_s-coupled DA receptor, Dop1R1, expressed in KCs. 21,22 Since one of the classical learning mutant genes identified by genetic screen was rutabaga (rut), which encodes Ca2+-dependent adenylate cyclase abundantly expressed in KCs, 23-25 it is believed that coincidence of odorevoked Ca2+ influx in KCs and DA input triggers cyclic adenosine monophosphate (cAMP)-dependent plasticity.²⁶ Indeed, KC activation and DA application can synergistically elevate cAMP level in KC axons in a rut-dependent manner.²⁷ Furthermore, simultaneous activation of KCs and DANs can induce robust long-term depression (LTD) at KC to MB output neuron (MBON) synapses, and the plasticity induction strictly depends on the temporal sequence of KC and DAN activity.5

Just like pyramidal neurons of the olfactory cortex, KCs show sparse responses to odors.31,32 The sparseness of the KC response depends at least in part on a single, key inhibitory neuron in the MB called anterior paired lateral (APL) neuron.³ Impairment of sparse coding by inactivating APL neuron causes learning defects, demonstrating that sparse coding at KCs is essential for stimulus-specific learning. 33,34 However, sparse coding alone is not enough to prevent unspecific association. First, there are significant overlaps between representations of odors whether they are chemically related.³⁵ The degree of such overlap directly correlates with the degree of crosstalk in plasticity.⁵ Second, although, on average, only about 5% of KCs reliably respond to multiple presentations of a given odor, there are up to 15% additional KCs that unreliably respond in a given trial.³² Those unreliable responders show smaller Ca²⁺ responses than the reliable ones.³² Although the former phenomena (i.e., reliable overlap) could be beneficial for animals by contributing to biologically important generalization across stimuli. 5,35 the latter (i.e., unreliable overlap) will be only detrimental for learning by causing unspecific learning. This is important because DA-induced plasticity at KC-MBON synapses is so effective that even a single, brief odor-DA pairing can induce a long-lasting change in odor responses in some MBONs.5,28,29 Furthermore, despite the prevailing model of coincidence detection of Ca2+ and DA signals by Rutabaga, DA alone can elevate cAMP level in KCs to some extent even without activation of KCs.^{27,36} These considerations prompted us to search for additional mechanisms at synaptic terminals to prevent unspecific

Recently reported ultrastructural connectomics of the MB circuit revealed that there are surprisingly large numbers of KC-KC connections. In fact, more than 80% of local synaptic inputs to the KC axons are provided by the cholinergic KCs themselves.²⁰ Since no excitatory role was found for acetylcholine (ACh) in KC axons,37 it suggests that ACh most likely acts as a neuromodulator rather than fast excitatory neurotransmitter. Although ACh is the main excitatory neurotransmitter in the *Drosophila* brain, its modulatory action has been understudied. The Drosophila brain expresses only two types of metabotropic muscarinic ACh receptors: mAChR-A, coupled to Ga, and mAChR-B, coupled to G_{i/o}. ^{38,39} Because of the distinct downstream pathways, genetic manipulations of one of the receptors do not result

in functional compensation by the other. Furthermore, mAChR-A is expressed only in KC dendrites, 40 suggesting a possible role for mAChR-B in KC-KC axonal neuromodulation.

Here, we show that KC-KC axonal interaction is mediated by mAChR-B. This mAChR-B-mediated neuromodulation has two roles: it decreases both odor-evoked Ca2+ elevation and DAinduced cAMP elevation. Thus, this neuromodulation acts to reduce both signals that are required for KC-MBON synaptic plasticity. We further show that knocking down mAChR-B results in unspecific learning. That is, an odor that was not coupled to a punishment signal is perceived as being coupled to one. We therefore suggest that active KCs release ACh on cognate KCs that are less or non-active. This lateral neuromodulation enhances stimulus specificity of learning.

RESULTS

γ KCs have extensive lateral axo-axonal connections

Our central hypothesis is that abundant axonal interactions between KCs mediate essential neuromodulation for learning. We therefore used the recently published Drosophila brain connectome⁴¹ to examine KC-KC interactions. Our goal was to uncover which type of KCs has the most lateral connections and to examine the cellular compartment in which these lateral KC-KC connections occur. As expected, almost no KC-KC interactions are observed between dendrites, and the vast majority of KC-KC interactions are between axons (Figure S1A). There are three types of KCs ($\alpha\beta$, $\alpha'\beta'$, and γ), which are defined according to their innervation pattern. 17,18 $\alpha\beta$ and $\alpha'\beta'$ KCs bifurcate and send axons to the vertical (α and α') and horizontal (β and β') lobes, whereas γ KCs send axons only to the horizontal γ lobe. These different KCs play different roles in olfactory learning.^{26,42} KC-KC interactions were mostly limited to within-subtypes (Figure S1A). γ KCs showed the most robust connectivity, with each KC synapsing on average with 190 other KCs, whereas $\alpha\beta$ and $\alpha'\beta'$ synapsed on average on 145 and 109 KCs, respectively (Figures S1B and S1C).

mAChR-B is expressed in γ KC axonal terminals

Recently, KCs were found to be cholinergic.³⁷ It has been also suggested that KC axons are essentially devoid of nicotinic receptors, as local application of ACh or nicotine on KC axons generated no Ca2+ signal.37 Although we recently showed that mAChR-A is expressed in KCs, it is localized at the dendrites.⁴ As the fly brain only expresses two muscarinic receptors, 43,44 mAChR-B is the most logical candidate to mediate KC-KC axonal interactions. We therefore first examined which types of KCs express mAChR-B. To this end, we used two driver lines that can express GAL4 wherever mAChR-B is endogenously expressed; one is from the Minos-mediated integration cassette (MiMIC) collection⁴⁵ and the other from the collection of T2A-GAL4 knockins. 46 The MiMIC insertion resides in the 5' untranslated region of the mAChR-B gene, and we used recombinasemediated cassette exchange (RMCE) to replace the original MiMIC cassette that contains GFP with a MiMIC cassette containing GAL4⁴⁵ to generate a new mAChR-B-MiMIC-GAL4 driver line. In the case of the mAChR-B-T2A-GAL4 knockins, the T2A-GAL4 cassette is inserted immediately upstream of the mAChR-B stop codon. Enhancer-driven eGFP expression using

Article



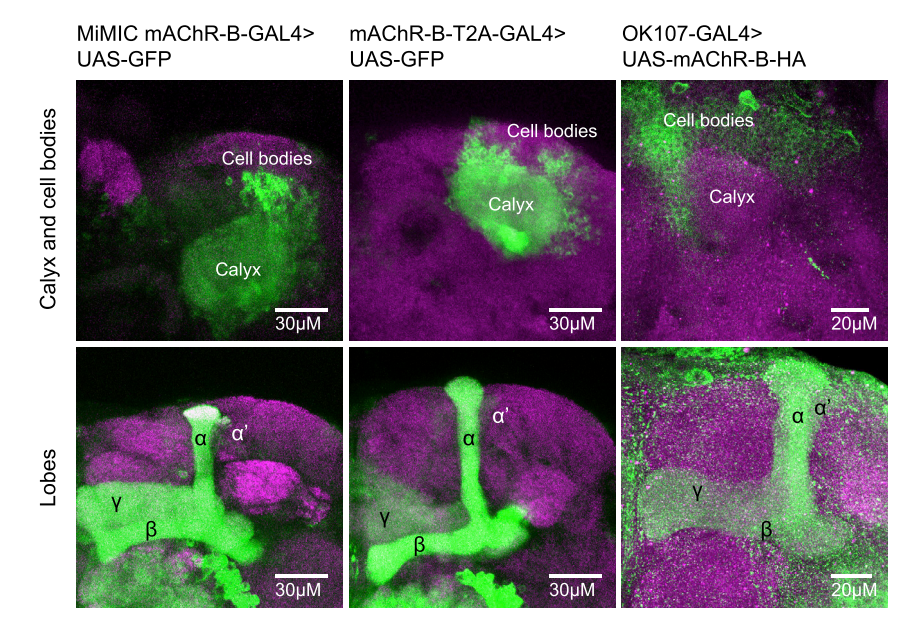


Figure 1. mAChR-B expression pattern

Maximum intensity projection of confocal sections through the central brain of a fly carrying MiMICmAChR-B-GAL4 (left) or mAChR-B-T2A-GAL4 (middle) and UAS-GFP transgenes. MB $\alpha\beta$ and γ lobes are clearly observed (bottom, 80 and 71 confocal sections, respectively, 1 µm). Very weak GFP expression is observed in $\alpha'\beta'$ lobes. As expected from soluble GFP labeling, the calyx is clearly observed (top, 44 and 24 confocal sections, respectively, 1 μm). Right: the pan-KC driver, OK107-GAL4, was used to overexpress UASmAChR-B-HA (with an HA tag). Although KC axons at the MB lobes are clearly visible (bottom, 43 confocal sections, 0.5 $\mu\text{m})\text{, there is no expression at}$ the calyx (compare with left and middle panels, 44 confocal sections, 0.5 μ m), indicating that mAChR-B is normally expressed in the axonal compartment.

See also Figure S1 and Data S1.

those two independent lines was evident in $\alpha\beta$ and γ but not in $\alpha'\beta'$ KCs (Figure 1). Consistent with these results, single-cell or cell type-specific transcriptomic analyses of the Drosophila brain^{43,44,47} suggest that mAChR-B is expressed more strongly in $\alpha\beta$ and γ than in $\alpha'\beta'$ KCs (Figures S1D–S1F). To determine which subcellular compartments express mAChR-B, we generated a transgene of UAS-mAChR-B tagged with the hemagglutinin (HA) tag in its C-terminal and used the pan-KC driver line. OK107-GAL4. Overexpression of mAChR-B-HA revealed expression in the axonal lobes and cell bodies but not in the dendrites at the calyx (Figure 1). These results suggest that in the MB, mAChR-B is preferentially expressed in the axons of $\alpha\beta$ and γ KCs.

mAChR-B expression in KCs is required for efficient aversive olfactory learning

To test our central hypothesis, we next examined whether mAChR-B is required for aversive associative olfactory conditioning. To this end, we knocked down mAChR-B expression using one of two UAS-RNAi lines, "RNAi 1" or "RNAi 2," the latter of which required co-expression of Dicer-2 (Dcr-2) for optimal knockdown (KD). To evaluate the RNAi efficiency, we performed quantitative real-time PCR. We knocked down mAChR-B expression using the pan-neuronal driver elav-GAL4. Both RNAi 1 and RNAi 2 significantly reduced mAChR-B levels to about 55% and 25% of the original mAChR-B level (Figure S2A). To knock down mAChR-B in KCs, we used the pan-KC driver OK107-GAL4. Short-term aversive memory was examined using two odors, 4-methylcyclohexanol (MCH) and 3-octanol (OCT), which are standard in the field. 48 For both UAS-RNAi transgenes, similar reduction in memory performance was observed, whether training was against MCH or OCT (Figure 2A). To verify that the reduced learning does not arise from defects in odor or electric shock perception, we examined naive odor valence and preference as well as reaction to electric shock. Both UAS-RNAi transgenes had no effect on these properties (Figures S2B–S2D). To rule out the possibility that developmental effects may

underlie the learning defect observed in mAChR-B KD flies, we used tub-GAL80^{ts} to suppress RNAi 1 expression during development. GAL80ts blocks the GAL4 transcription factor at 23°C but allows for normal expression of the UAS transgene at 31°C.⁴⁹ Flies were grown at 23°C until post-eclosion to block RNAi expression and allow for normal development and were then transferred to 31°C for 7 days to allow for the RNAi to be expressed and take effect. KD of mAChR-B only at the adult stage recapitulated the effect of constitutive KD of mAChR-B (Figure 2B). As a control to verify that GAL80ts efficiently blocks RNAi expression, flies were constantly grown at 23°C (i.e., without transferring them to 31°C), thus blocking the RNAi expression also in adult flies. These flies showed normal olfactory associative learning (Figure 2B). Together, these results indicate that mAChR-B has a physiological role in associative olfactory aversive conditioning.

mAChR-B is required for olfactory learning in γ KCs, but not in $\alpha\beta$ or $\alpha'\beta'$ KCs

Following the expression pattern of mAChR-B that is limited to $\alpha\beta$ and γ KCs (Figure 1), we sought to examine in which KCs mAChR-B has a role in olfactory learning. To this end, we knocked down mAChR-B expression using RNAi 1 in different KC subtypes. As expected from the anatomical expression pattern of mAChR-B (Figure 1), aversive olfactory conditioning was impaired when mAChR-B was knocked down in $\alpha\beta$ and γ KCs using MB247-GAL4, but not by KD in $\alpha'\beta'$ KCs using c305a-GAL4 (Figure 2C). To examine if mAChR-B is required for aversive olfactory conditioning in both $\alpha\beta$ and γ KCs, we used R28H05-GAL4 and R71G10-GAL4 lines, which drives expression only in $\alpha\beta$ KCs or in γ KCs, respectively. Aversive olfactory conditioning was impaired when mAChR-B was knocked down in γ , but not in $\alpha\beta$, KCs (Figure 2C). The combined expression pattern, anatomical connectivity, and behavioral results all point to a role of mAChR-B in the context of aversive olfactory conditioning, specifically in γ KCs axons.



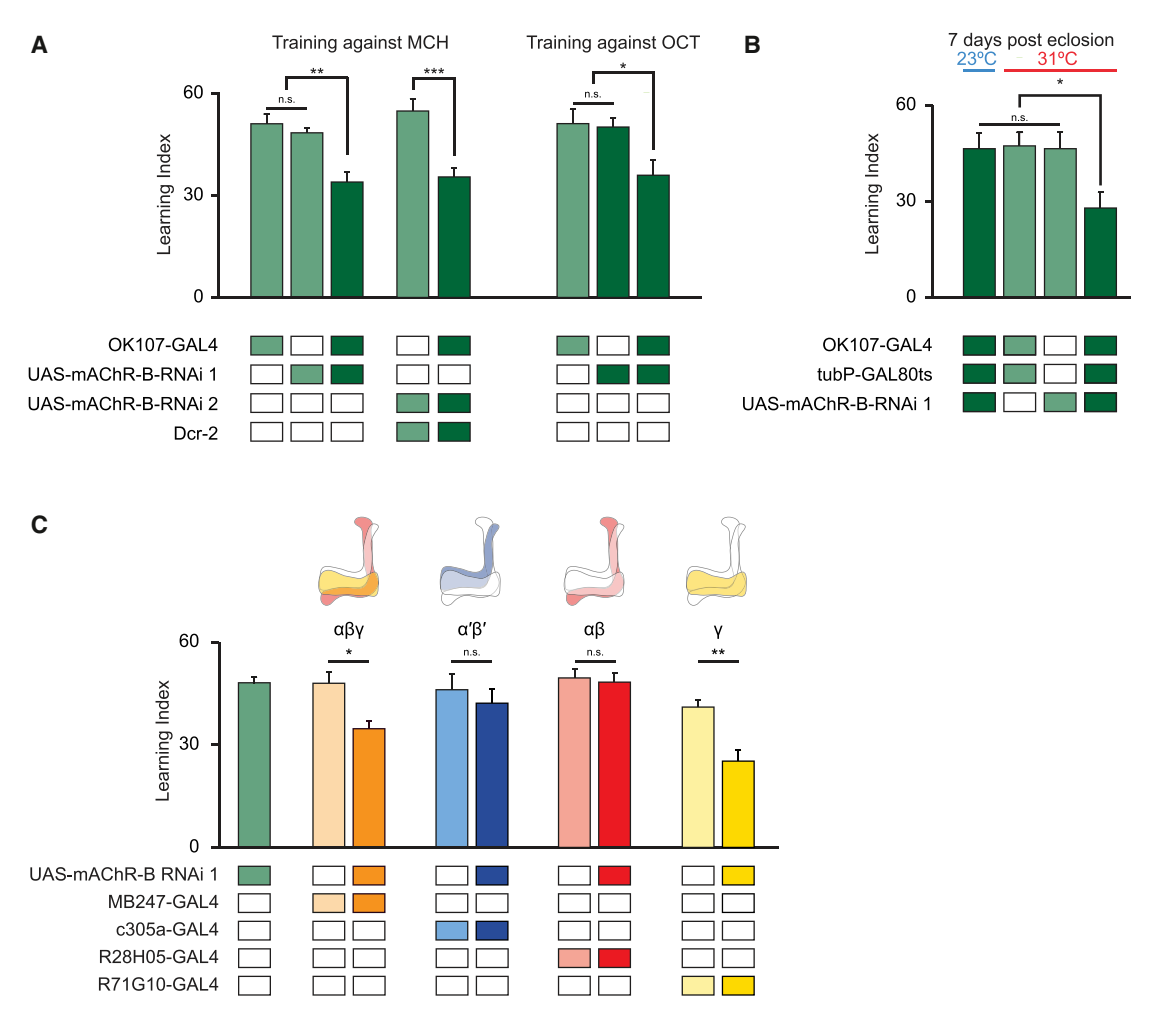


Figure 2. mAChR-B is required in γ KCs for short-term aversive olfactory learning

(A) Learning scores in flies with mAChR-B RNAi 1 or 2 driven by OK107-GAL4. mAChR-B KD reduced learning scores compared with controls (mean \pm SEM). n (left to right): 49, 162, 77, 66, 61, 60, 63, 51; *p < 0.05, **p < 0.01, ***p < 0.001 (Kruskal-Wallis with Dunn's correction for multiple comparisons). For detailed statistical analysis, see Table S1.

(B) Learning scores in flies with mAChR-B RNAi 1 driven by OK107-GAL4 with GAL80^{ts} repression. Flies raised at 23°C and heated to 31°C as adults (red horizontal bar) had impaired learning compared with controls. Control flies kept at 23°C throughout (blue horizontal bar), thus blocking mAChR-B RNAi expression, showed no learning defects (mean ± SEM). n (left to right): 63, 60, 69, 61; *p < 0.05, **p < 0.01, ***p < 0.001 (Kruskal-Wallis with Dunn's correction for multiple comparisons). For detailed statistical analysis, see Table S1.

(C) mAChR-B RNAi 1 was targeted to different subpopulations of KCs using c305a-GAL4 ($\alpha'\beta'$ KCs), MB247-GAL4 ($\alpha\beta\gamma$ KCs), R28H05-GAL4 ($\alpha\beta$ KCs), and R71G10-GAL4 (γ KCs). Learning scores were reduced compared with controls when mAChR-B RNAi 1 was expressed in $\alpha\beta$ and γ KCs or γ KCs alone, but not when mAChR-B RNAi 1 was expressed in $\alpha\beta$ or $\alpha'\beta'$ KCs (mean \pm SEM). n (left to right): 162, 73, 70, 54, 61, 72, 60, 91, 69; *p < 0.05, **p < 0.01 (Kruskal-Wallis with Dunn's correction for multiple comparisons). For detailed statistical analysis, see Table S1. The data for the UAS-mAChR-B RNAi 1 control are duplicated from (A).

See also Figure S2, Data S1, and Table S1.

mAChR-B suppresses odor responses only in γ KC axons

To gain mechanistic understanding of the role played by mAChR-B in olfactory learning, we next examined whether mAChR-B contributes to olfactory responses in KCs. To this end, we expressed the genetically encoded Ca²⁺ indicator, GCaMP6f, with or without mAChR-B RNAi 1 using MB247-GAL4 (labels $\alpha\beta$ and γ KCs), c305a-GAL4 (labels $\alpha'\beta'$ KCs), or R71G10-GAL4 (labels only γ KCs) and examined, using *in vivo* 2-photon functional imaging, the effect mAChR-B KD has on responses to MCH and OCT. To check for various effects on the odor response, we examined three different parameters: the

peak of the "on" and "off" responses and the overall strength of the odor response as measured by the integral of the response (STAR Methods). Following mAChR-B KD, we found a significant and reliable increase in odor responses in γ KCs (Figure 3). The increase was observed in all three parameters. Importantly, consistent with our observation that mAChR-B is expressed in the axons, no effect was observed in the dendritic arborizations in the calyx. This was true for both the broad MB247-GAL4 driver line and the γ -KC-specific driver line, R71G10-GAL4 (Figure 3). The fact that no effect was observed in KC dendritic arborization (Figure 3) indicates that KC recruitment by upstream projection

Article



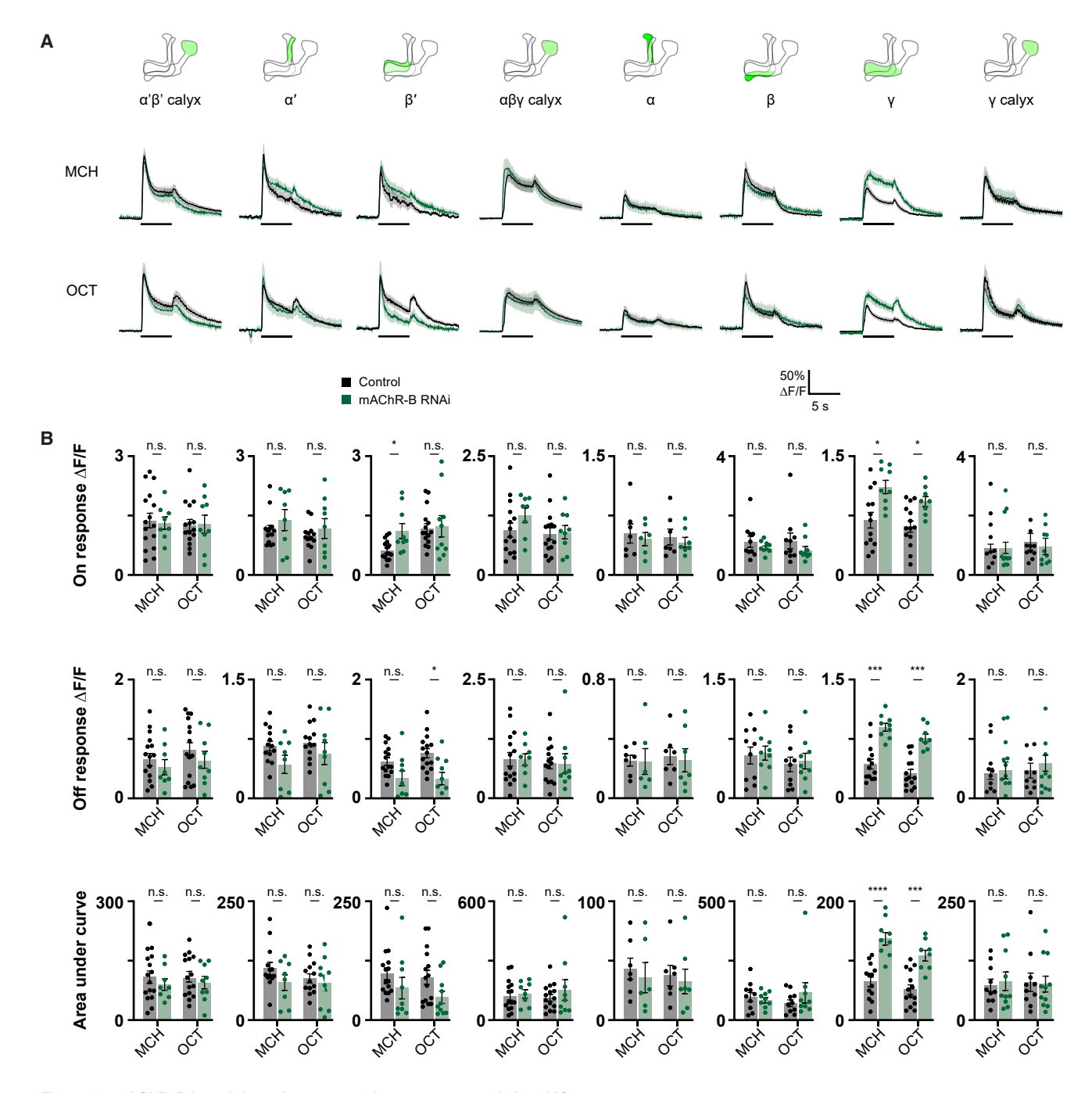


Figure 3. mAChR-B knockdown increases odor responses only in γ KC axons

Odor responses to MCH and OCT were measured in control flies (GAL4>UAS-GCaMP6f) and knockdown flies (GAL4>UAS-GCaMP6f, UAS-mAChR-B RNAi 1). The following driver lines were used: c305a-GAL4 (α/β/ KCs), MB247-GAL4 (α/βγ KCs), and R71G10-GAL4 (labels only γ KCs).

(A) Δ F/F of GCaMP6f signal in different areas of the MB in control (black) and knockdown (green) flies, during presentation of odor pulses (horizontal lines). Data are mean (solid line) \pm SEM (shaded area). Diagrams illustrate which region of the MB was analyzed.

(B) Peak "on" response (top), peak "off" response (middle), and the integral of the odor response (bottom) of the traces presented in (A) (mean ± SEM). Only in γ KC axons is a significant increase in odor responses observed. This increase was observed for both odors and in all modes of analysis. n for control MCH, OCT, and KD MCH OCT flies, respectively: $\alpha'\beta'$ calyx, 16, 15, 8, 9; α' , 13, 13, 8, 9; β' , 15, 15, 9, and 10; $\alpha\beta\gamma$ calyx, 15, 15, 8, 9; α , 7, 7, 6, 7; β , 10, 10, 9, and 9; γ , 13, 14, 9, and 8; γ calyx, 10, 10, 10, and 11. *p < 0.05, ***p < 0.001, ****p < 0.0001 (Mann-Whitney test with Holm Šídák correction for multiple comparisons). For detailed statistical analysis, see Table S1.

See also Figure S3, Data S1, and Table S1.



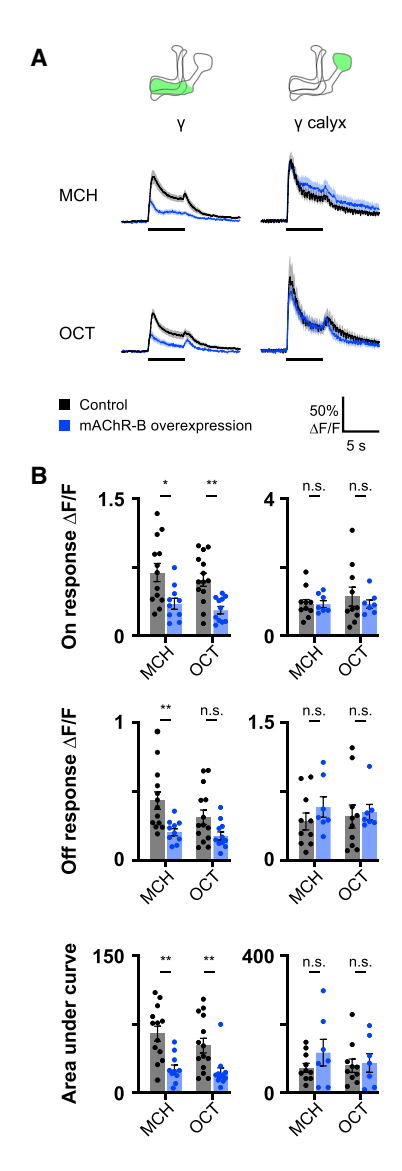


Figure 4. mAChR-B overexpression decreases odor responses only

Odor responses to MCH and OCT were measured in control flies (R71G10-GAL4>UAS-GcaMP6f) and overexpression flies (R71G10-GAL4>UAS-GcaMP6f, UAS-mAChR-B).

(A) Δ F/F of GCaMP6f signal in the calyx and lobe of γ KCs for control (black) and overexpression (blue) flies, during presentation of odor pulses (horizontal lines). Data are mean (solid line) ± SEM (shaded area). Diagrams illustrate which region of the MB was analyzed.

(B) Peak "on" response (top), peak "off" response (middle), and the integral of the odor response (bottom) of the traces presented in (A) (mean \pm SEM). Only in γ KC axons is a significant decrease in odor responses observed. This decrease was observed for both odors and in all modes of analysis. n for control MCH, OCT, and overexpression MCH OCT flies, respectively: γ , 14, 13, 10, and 11; γ calyx, 10, 10, 7, and 7. *p < 0.05, **p < 0.01 (Mann-Whitney test with Holm Šídák correction for multiple comparisons). For detailed statistical analysis, see Table S1.

See also Data S1 and Table S1.

neurons is not impaired by mAChR-B KD and that mAChR-B neuromodulation occurs locally at KC presynaptic axonal terminals. To test whether the observed increase in Ca2+ response affects synaptic release, we used the genetically encoded ACh sensor, ACh3.0⁵¹ that reports ACh level in the synaptic cleft. We expressed ACh3.0 in KCs using the MB247-GAL4 driver line and examined KC synaptic release following odor application (MCH and OCT). Consistent with the above result, a significant increase of all three examined parameters (as above), except for OCT off response, was observed also for released ACh levels (Figure S3).

We next examined whether overexpression of mAChR-B has an opposite effect to that of mAChR-B KD. To this end, we generated a UAS-mAChR-B transgene and used R71G10-GAL4 to drive mAChR-B in γ KCs. To verify the efficiency of the UAS-mAChR-B overexpression, we used the pan-neuronal driver elav-GAL4 to overexpress mAChR-B and examined its level using quantitative real-time PCR. Overexpression of mAChR-B resulted in increased levels of about 155% relative to the original level (Figure S2A). As expected from the above results (Figures 1 and 3), overexpression of mAChR-B resulted in decreased odor-evoked Ca^{2+} response in γ KCs axons but not in the dendritic arborization, except for OCT off response (Figure 4). Taken together, these results suggest that mAChR-B normally acts to reduce the odor-evoked Ca²⁺ response and synaptic output at γ KC axons.

mAChR-B suppresses dopamine-induced increase in **cAMP**

Studies in heterologous expression systems suggested that mAChR-B is coupled to G_{i/o}.^{38,39} Hence, we next examined whether ACh application on KCs affects cAMP level. To this end, we used MB247-GAL4 to drive expression of the recently developed genetically encoded cAMP indicator, cAMPr. 52 We used tetrodotoxin (TTX) to block circuit effects and locally applied 1 mM ACh using a puff pipette targeted to KC axons at the horizontal lobe. We observed that ACh application significantly reduces cAMP level (Figure 5A, black). To verify that this reduction indeed arises from activation of mAChR-B expressed in KCs, we repeated the experiment but with mAChR-B KD in KCs using RNAi 1. KD of mAChR-B almost completely suppressed the reduction in cAMP level (Figure 5A, green). Thus, even if there were residual circuit effects in the presence of TTX (e.g., via the APL neuron), KD of mAChR-B in KCs should not have affected these residual effects. Together, the effect of mAChR-B KD in KCs clearly indicates that the net effect of ACh on cAMP signaling in KCs is inhibitory and that it is mediated by mAChR-B.

DA exerts its main effect on aversive olfactory conditioning by activation of Dop1R1, which is Gs coupled, and increases cAMP level.^{27,36} We therefore examined whether activation of mAChR-B can counter the effect of DA application on cAMP level. As before, MB247-GAL4 was used to drive cAMPr, and TTX was used to block any circuit effects. DA at high concentration (5 mM) was bath applied and generated a robust and sustained elevation in cAMP level (Figure 5B, red). Local application of ACh significantly reduced cAMP to the initial basal level (Figure 5B, black). To verify that this reduced level of cAMP indeed arises from mAChR-B activation, we knocked down mAChR-B in KCs using RNAi 1. Under these conditions, ACh application had little effect on cAMP level (Figure 5B, green). Together, these results indicate that mAChR-B can counter the DA-induced increase in cAMP by reducing cAMP level.

Article



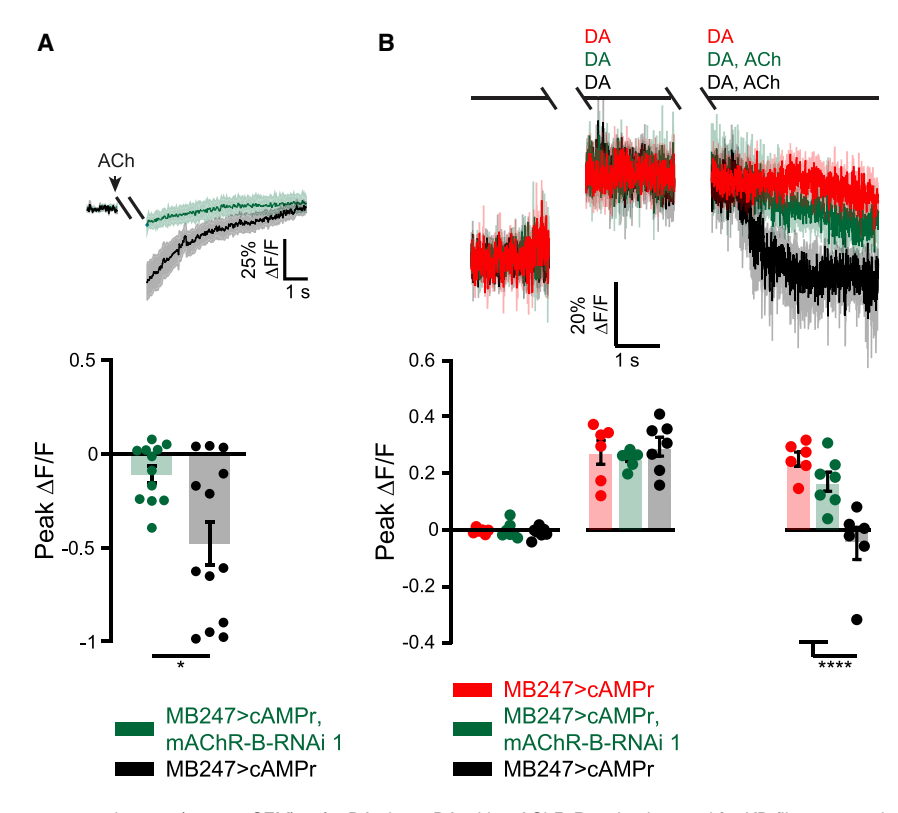


Figure 5. mAChR-B decreases cAMP level

cAMP level was measured using the single-wavelength fluorescent sensor for cyclic AMP, UAS-cAMPr. MB247-GAL was used to drive expression.

(A) Top: Δ F/F of cAMPr following activation of mAChR-B using a 2 s puff (gap) of 1 mM Ach (black). To abolish any circuit effects, 1 μ M TTX was bath applied. KD of mAChR-B using UAS-mAChR-B RNAi 1 (green) abolished the decrease in cAMP, indicating that the observed cAMP decrease indeed arises from mAChR-B activation. Data are mean (solid line) \pm SEM (shaded area). Bottom: peak response of the top presented traces (mean \pm SEM). n for WT and KD flies, respectively, 13, 12; *p < 0.05 (Mann-Whitney two-tailed rank test). For detailed statistical analysis, see Table S1.

(B) Top: Δ F/F of cAMPr. Application of 5 mM DA resulted in sustained increase in cAMP levels (red). The 2 s gap is when a puff of DA was given and either DA or ACh and DA together was given. Activation of mAChR-B using a puff of 0.5 mM ACh (black) significantly decreased cAMP levels to the initial level. To abolish any circuit effects, 1 μ M TTX was bath applied. KD of mAChR-B using UAS-mAChR-B RNAi 1 (green) resulted in almost no decrease of cAMP indicating that the observed cAMP decrease indeed arises from mAChR-B activation. Data are mean (solid line) \pm SEM (shaded area). Bottom: peak response of the top

presented traces (mean ± SEM). n for DA alone, DA with mAChR-B activation, and for KD flies, respectively, 7, 6, 7; ****p < 0.0001 (Shapiro-Wilk normality test, followed by two-way ANOVA with Tukey's correction for multiple comparisons). For detailed statistical analysis, see Table S1.

See also Data S1 and Table S1.

mAChR-B mediates lateral KC neuromodulation

The results thus far demonstrate that mAChR-B can counter both signals required for efficient plasticity in KC presynaptic axonal terminals: Ca²⁺ and cAMP elevation. We now turn to examine the source of ACh that activates KC mAChR-B. The vast KC-KC axonal interactions (Figures S1A–S1C) suggest that KCs are the source of the ACh. We therefore used MB247-GAL4 to express the tetanus toxin light chain (TNT), which inhibits synaptic transmission.⁵³ Blocking KC synaptic release abolished the effect of mAChR-B KD on odor-evoked Ca²⁺ responses (Figures S4A and S4B), suggesting that KCs are the source of the ACh that attenuate odor-evoked Ca²⁺ responses in normal flies.

The existence of lateral KC-KC axonal interactions and axonal localization of mAChR-B suggest that KCs affect other, neighboring KCs via mAChR-B. However, mammalian muscarinic M2 that is also coupled to G_{I/o} often acts as an autoreceptor. ^{54,55} Therefore, to examine whether mAChR-B promotes lateral neuromodulation, we sought to activate a subpopulation of KCs and examine how synaptic release from this subpopulation affects odor responses in other cognate KCs (Figure 6A). To this end, we used the recently developed sparse predictive activity through recombinase competition (SPARC) method ⁵⁶ to express the red-light-activated channel, CsChrimson, ⁵⁷ in a subpopulation of KCs, thus allowing for their optogenetic activation (Figure 6A). Specifically, we used the intermediate variant of SPARC2 (SPARC2-I)-CsChrimson::tdTomato, which is expected to achieve expression in approximately 17%–22% of the

targeted neurons, 56 together with MB247-GAL4 and pan-neuronally expressed nSyb-PhiC31 to express CsChrimson in a small subset of $\alpha\beta$ and γ KCs. GCaMP6f was expressed in all $\alpha\beta$ and γ KCs using MB247-LexA and LexAop-GCaMP6f (Figure 6B). This experimental configuration allows us to examine how activation of a subpopulation of KCs affects odor responses of other KCs (Figure 6A). To ensure that only lateral effects are measured, we examined odor responses only in γ KCs that did not express CsChrimson (Figure S4C; STAR Methods). KC odor responses were examined with and without optogenetic activation (Figure 6A). To normalize the potential effects of repeated presentations of the same odor, we presented the odor pulse without opotogentic activation first in half of the experiments and vice versa in the other half. Consistent with the inhibitory effect mAChR-B had on γ KC odor responses (Figures 3 and 4), optogenetic activation of the CsChrimson resulted in decreased odor responses in CsChrimson-negative γ KCs, demonstrating a lateral suppression of KC activity (Figures 6C-6H). Furthermore, consistent with the above results (Figures 3 and 4), this lateral suppression was completely abolished with mAChR-B KD in γ KCs (and $\alpha\beta$ KCs which are also labeled by MB247-GAL4; Figures 6I-6N). Thus, these results demonstrate that mAChR-B mediates lateral KC-KC neuromodulation. It is important to note, although, that mAChR-B can still also function as an autoreceptor.

mAChR-B decreases unspecific learning

How can the physiological actions of mAChR-B we demonstrated so far explain the impaired learning in mAChR-B KD flies



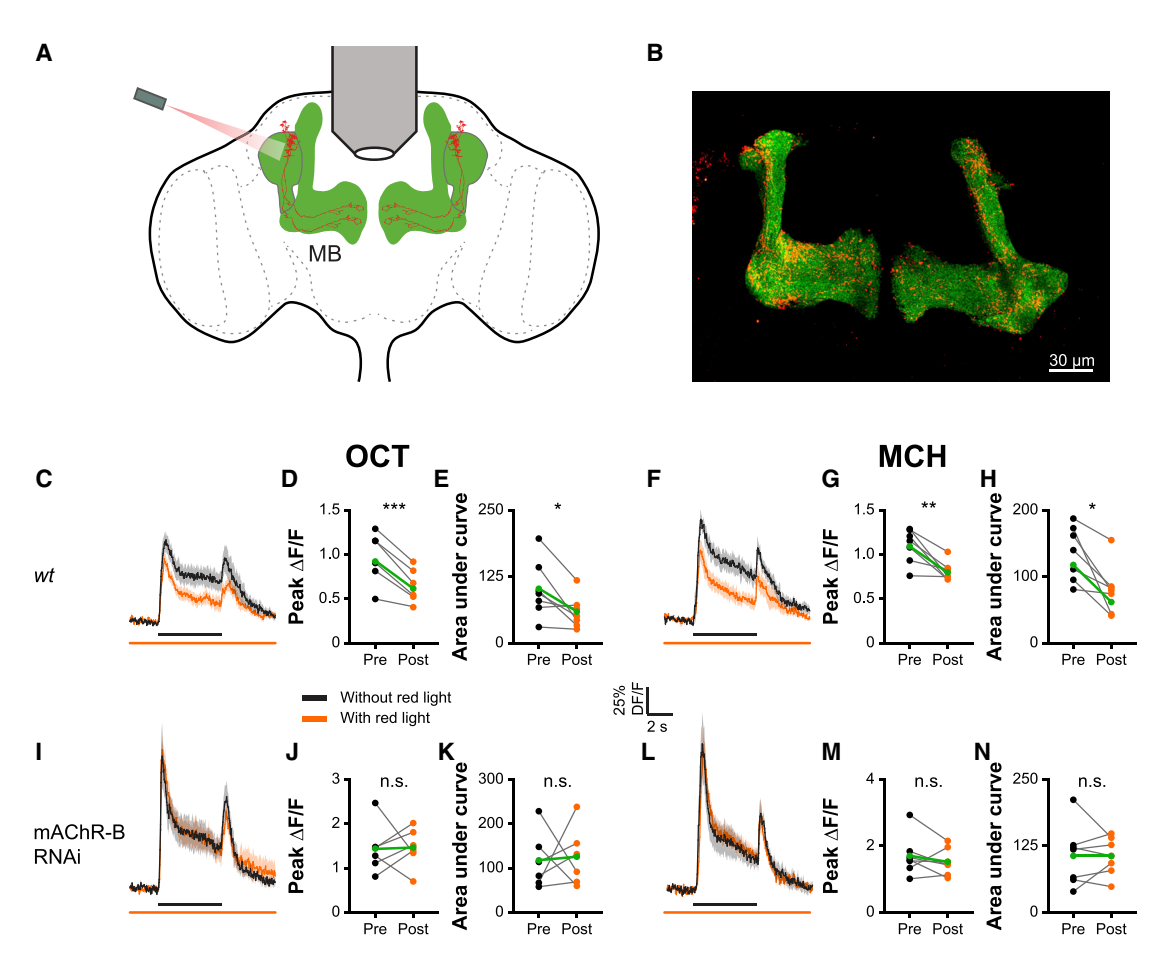


Figure 6. Axo-axonal lateral neuromodulation underlies mAChR-B effects

(A) Experimental configuration. GcaMP6f was expressed in all αβγ KCs. The SPARC method was used to drive CsChrimson in a small subset of αβγ KCs. Responses to MCH and OCT of \(\gamma \) KCs that do not express CsChrimson were examined with and without optogenetic activation of the KC subpopulation. (B) Example of a fly brain with the strategy presented in (A). Maximum intensity projection of 28 confocal sections (1 µm) through the central brain of a fly carrying MB247-LexA-LexAop-GcaMP6f, and CsChrimson::tdTomato in stochastically distributed subsets of neurons within the MB247-GAL4 driver line transgenes. (C, F, I, and L) ΔF/F of GCaMP6f signal in the γ KC lobe for control (C and F) and KD (I and L) flies, during presentation of odor pulses (OCT, C and I; MCH, F and L; horizontal black lines) without (black) or with (orange) optogenetic activation of the KC subpopulation expressing CsChrimson. MB247-LexA was used to drive LexAop-GcaMP. MB247-GAL4 was used to drive UAS-mAChR-B RNAi 1 and TI{20XUAS-SPARC2-I-Syn21-CsChrimson::tdTomato-3.1}CR-P40. Data are mean (solid line) ± SEM (shaded area). GCaMP signals were taken from regions not expressing CsChrimson (see Figure S4C). (D, E, G, H, J, K, M, and N) Peak "on" response (D, G, J, and M) and the integral of the odor response (E, H, K, and N) of the traces presented in (C), (F), (I), and (L) before (left) or after (right) optogenetic activation. A significant decrease in odor responses is observed only in control flies, indicating lateral neuromodulation. This lateral neuromodulation is absent in KD flies not expressing mAChR-B. n for control and KD flies, respectively: OCT, 7, and 6; MCH, 7, 7, *p < 0.05, **p < 0.01, ***p < 0.001 (Wilcoxon matched-pairs signed-rank test). For detailed statistical analysis, see Table S1. See also Figure S4, Data S1, and Table S1.

(Figure 2)? In the MB, coincidence of KC activity (i.e., Ca2+ increase), which represents olfactory signal, and DA input (i.e., cAMP increase), which represents reinforcement signal, is considered to induce synaptic plasticity and learning. If mAChR-B in KCs acts synergistically with the DA signaling pathway, then this could explain the impaired learning in mAChR-B KD flies (i.e., defective learning). However, our results show antagonistic actions of ACh and DA in KCs (Figure 5), which makes this scenario unlikely. As an alternative scenario, we hypothesized that lateral KC-KC interactions mediated by mAChR-B may prevent unspecific learning by suppressing both Ca²⁺ and cAMP increase in less active or inactive KCs during conditioning. These two scenarios predict entirely different

types of learning impairment (i.e., defective versus unspecific learning; Figure S5) in mAChR-B KD flies with respect to the valence change in paired odor (conditioned stimulus, CS+) and unpaired, control odor (CS-). That is, in defective learning, the negative shift of the valence of CS+ after aversive learning should be diminished (Figure S5C), whereas in unspecific learning, the valence shift of CS+ should not be affected, but CS- should show more negative shift than normal (Figure S5D).

To discriminate these possibilities, flies were conditioned against MCH (i.e., MCH was coupled with an electric shock), and the valence of either MCH or OCT was examined by measuring the preference of the odor against mineral oil (Figure 7A; STAR Methods). Note that OCT is a novel odor for flies

Article



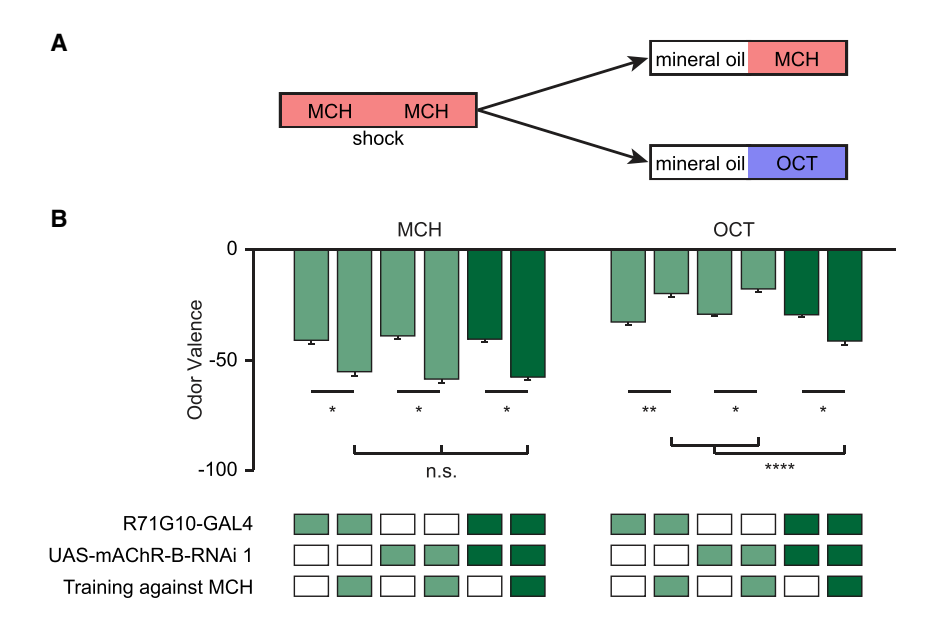


Figure 7. mAChR-B KD results in unspecific conditioning

(A) Experimental protocol. Flies were conditioned against MCH using 12 equally spaced 1.25 s electric shocks at 50 V. Flies were then subjected to OCT or MCH for valence evaluation (STAR Methods).

(B) MCH or OCT valence (as designated) observed with or without pre-exposure to conditioning against MCH in flies with mAChR-B RNAi 1 driven by R71G10-GAL4 (γ KCs). Following conditioning against MCH, both mAChR-B KD and control flies showed the same increase in aversion toward MCH. In contrast, when OCT valence was examined. mAChR-B KD flies showed increased aversion toward OCT, whereas the parental controls showed reduced aversion toward OCT (mean ± SEM), n (left to right): MCH: 63, 61, 65, 70, 73, and 75; OCT: 96, 76, 66, 77, 101, and 76; *p < 0.05, **p < 0.01, ***p < 0.001 (Kruskal-Wallis Dunn's correction for multiple comparisons). For detailed statistical analysis, see Table S1.

See also Figures S5-S7, Data S1, and Table S1.

in this assay. As expected, following aversive conditioning against MCH, MCH became more aversive than it was before (Figure 7B). For the parental control flies, following aversive conditioning against MCH, OCT became slightly more attractive (Figure 7B). In agreement with our findings that mAChR-B opposes DA neuromodulation and that KCs exert lateral neuromodulation on cognate KCs, KD of mAChR-B had no effect on the increase in aversion toward MCH (Figure 7B). However, the change in OCT valence reversed, and rather than becoming more attractive, OCT became more aversive (Figure 7B). These results were also repeated with another odor pair, MCH and isopentyl acetate (IPA, Figures S6A and S6B). Taken together, these results are consistent with the unspecific learning model suggested above (Figure S5).

DISCUSSION

Here, we showed that KC-KC axonal interaction is mediated by mAChR-B. This mAChR-B-mediated neuromodulation has dual roles: it decreases both odor-evoked Ca2+ elevation and DAinduced cAMP elevation. Thus, this neuromodulation suppresses both signals that are required for KC-MBON synaptic plasticity. In behavior experiments, we demonstrated that mAChR-B KD in KCs impairs stimulus specificity of learning. Our study reveals a novel form of local neuromodulation, which improves sensory discrimination during learning.

In this study, we identified the first biological functions, to the best of our knowledge, of axo-axonic synapses between KCs. Olfactory coding in the insect MB is a well-established model system to study the circuit mechanisms and benefits of sparse sensory representations. The abundance of KC-KC synapses at the axons discovered by the EM connectome²⁰ surprised the field at first because excitatory cholinergic interactions may ruin the very benefit of the sparse coding in olfactory learning. However, our Ca²⁺ imaging demonstrated that the net effect of those cholinergic transmissions is, in fact, inhibitory. The lateral inhibition mediated by mAChR-B should further enhance, rather than ruin, the benefit of sparse coding and thereby improve the stimulus specificity of learning. Although the population of KCs that show reliable responses to a given odor is sparse (\sim 5%), many more KCs are activated in a given odor presentation. This is because there is a larger population of unreliable responders, making up to ${\sim}15\%$ of total KCs active in a given trial.³² Since those unreliable responders tend to show weaker Ca²⁺ responses than the reliable ones, it is reasonable to speculate that mAChR-B-mediated mutual inhibition would preferentially suppress unreliable responders, letting reliable responders win the lateral competition. Since even a single, 1-s odor-DAN activation pairing can induce robust KC-MBON synaptic plasticity,⁵ presence of unreliable responders can significantly compromise the synapse specificity of plasticity. Restricting Ca²⁺ responses to reliable responders should therefore greatly enhance the stimulus specificity of learning.

To support our finding, selective inhibition of Go signaling in KCs by expressing pertussis toxin (PTX) impairs aversive learning, and this effect was mapped to $\alpha\beta$ and γ KCs, ⁵⁸ which we found to express mAChR-B most abundantly. Furthermore, expression of PTX disinhibits odor-evoked vesicular release in γ KCs, and PTX-induced learning defect was ameliorated by hyperpolarization or blocking synaptic output of γ KCs.⁵⁹ We argue that mAChR-B-mediated inhibitory communication between γ KCs contributes at least in part to those previous observations.

Lateral communication through mAChR-B also suppresses cAMP signals in KCs, which counteracts Dop1R1-mediated DA action during associative conditioning. Since DA release in the MB likely takes a form of volume transmission, 20 it cannot provide target specificity of modulation. Furthermore, although induction of LTD depends on coincident activity of KCs and DANs, 5,28-30 elevation of cAMP can be triggered by DA application alone,²⁷ although DA input followed by KC activity could induce opposite plasticity (i.e., potentiation) via another type of DA receptor.²⁹ Thus, lateral inhibition of cAMP signals by G_{i/o}coupled mAChR-B plays an essential role in the maintenance of target specificity of modulation. Taken together, dual actions



Current Biology Article

of mAChR-B on local Ca2+ and cAMP signals at KC axons, where plasticity is supposed to take place, should directly contribute to synapse specificity of plasticity (Figure S7). If animals lack mAChR-B in KCs, axons of unreliable responders to CS⁺ would stay mildly active during conditioning. Furthermore, DA release on KCs causes some unchecked increase in cAMP in inactive and mildly active KCs. Consequently, some plasticity occurs in these KCs, even if to a lesser extent than in the KCs that are reliably and strongly activated by the CS+. Thus, absence of mAChR-B would minimally affect plasticity of KCs that are reliably activated by the CS+, assuming that those KCs are nearly maximally depressed by learning-related plasticity in the presence of mAChR-B. However, other KCs, which may include reliable responders to the CS-, will also undergo plasticity (Figure S7). This should result in unspecific association and that is exactly the type of learning defect we observed in mAChR-B KD flies (Figures 7 and S6).

The above model suggests that mAChR-B is required during memory acquisition. However, previous studies suggested that blocking KC synaptic output during memory acquisition does not affect aversive memory. 60-63 How can one reconcile these two seemingly contradictory results? Our experimental approach (i.e., RNAi KD of mAChR-B) precluded the ability to control the receptor function with high temporal specificity, and therefore, we could not directly test whether mAChR-B is required during memory acquisition. Nevertheless, we argue that it is plausible that KC output affects memory acquisition via mAChR-B. Previous literature relied on temperature-sensitive Shibire^{ts1} (shi^{ts1}), which blocks synaptic release at the restrictive temperature, to demonstrate that KC output is not required during memory acquisition. 60-63 However, it has been shown that substantial release is still maintained with shi^{ts1} even at the restrictive temperature. 33,64-66 GPCRs are known to be activated at extremely low concentrations, ranging in the nM.67,68 On the other hand, nicotinic receptors operate at higher concentrations, often in the range of μM . ^{69,70} Thus, it is possible that in the presence of shi^{ts1}, there is some residual release from KCs at the restrictive temperature that is sufficient to activate mAChR-B but not the nicotinic receptors on downstream neurons. Thus, our results shed light on the role of KC output during memory acquisition, which may have been overlooked in previous studies.

What may be the cellular mechanisms underlying the effects of mAChR-B on cAMP and Ca2+ level? mAChR-B was shown to be coupled to $G_{i/o}$, ³⁹ which is known to inhibit the cAMP synthase, adenylate cyclase,⁷¹ which is widely expressed in KCs.^{23,27} In addition, the $G_{\beta\gamma}$ subunits have been demonstrated to be able to directly block voltage-gated Ca^{2+} channels.⁷² $G_{\beta\gamma}$ can also directly open inward rectifying potassium channels⁷³ that would oppose the changes in membrane potential required for the gating of voltage-gated Ca2+ channels, although these potassium channels are not broadly expressed in KCs. 43,44,47 In this regard, it would be interesting to note that we observed behavioral and physiological effects of mAChR-B KD only when we performed KD in γ KCs, although our results indicate that those receptors are also expressed in $\alpha\beta$ KCs. This could be due to potential diversity in the intracellular signaling molecules among KC subtypes. Another possibility is that the efficiency of RNAi KD is somehow different between those KCs. It is also possible that

the relatively lower number of KC-KC connections between $\alpha\beta$ KCs may be insufficient to activate mAChR-B in our experimental contexts. Nevertheless, we note that a number of studies have demonstrated that γ KCs have a dominant role at the stage of acquisition of short-term memory, ^{22,74} which is consistent with our model that proposes the critical role of mAChR-B during memory acquisition.

Although the majority of study on population-level sensory coding has focused on somatic Ca2+ or extracellular electrophysiological recordings, our study sheds light on the importance of local regulation of Ca2+ and other intracellular signals at the axons when it comes to stimulus specificity of learning. Are there other mechanisms that may be involved in reducing unspecific conditioning? One potential source of such mechanisms is the APL neuron, a single GABAergic neuron in the MB that is excited by KCs and provides feedback inhibition to KCs. 33,75-77 Since activity of APL neuron contributes to sparse and decorrelated olfactory representations in KCs,33 it is possible that GABAergic input to KC axons also serves to prevent unspecific learning. Release of GABA onto KC axons is expected to have similar effects as the activation of mAChR-B. Specifically, the activation of the Gi/o-coupled GABA-B receptors that are widely expressed in $KCs^{43,44,47}$ should have similar effects as activation of mAChR-B. However, in our experiments, lateral inhibition induced by optogenetic activation of a subset of KCs was completely suppressed by mAChR-B KD (Figure 6), suggesting that APL neuron did not contribute to lateral suppression of Ca²⁺ response at least in our experimental condition. This result is consistent with the prediction that individual KCs inhibit themselves via APL neuron more strongly than they inhibit the others due to the localized nature of the activity of APL neuron's neurites and the geometric arrangement of the ultrastructurally identified synapses.⁷⁸ Nonetheless, whether APL neuron contributes to sparsening of axonal activity to prevent unspecific conditioning remains to be examined.

In summary, the current study identifies functional roles of axo-axonic cholinergic interactions by uncovering previously unknown local neuromodulation that can enhance the stimulus specificity of learning and refines the DA-centric view of MB plasticity.

STAR*METHODS

Detailed methods are provided in the online version of this paper and include the following:

- KEY RESOURCES TABLE
- RESOURCE AVAILABILITY
 - Lead contact
 - Materials availability
 - Data and code availability
- EXPERIMENTAL MODEL AND SUBJECT DETAILS
 - Fly strains
- METHOD DETAILS
 - Behavioral analysis
 - Functional imaging
 - Odors used
 - Optogenetic activation
 - Pharmacological application

Article



- Structural imaging
- O RNA purification, cDNA synthesis, and quantitative real-time PCR analysis
- O Connectome data analysis
- QUANTIFICATION AND STATISTICAL ANALYSIS
 - Statistics

SUPPLEMENTAL INFORMATION

Supplemental information can be found online at https://doi.org/10.1016/j. cub 2022 09 007.

ACKNOWLEDGMENTS

We thank the Bloomington Drosophila Stock Center (NIH P400D018537), the Vienna Drosophila RNAi Center, Dr. Andrew Lin (University of Sheffield), Dr. Justin Blau (New York University), and Dr. Oren Schuldiner (Weizmann Institute of Science) for providing Drosophila strains. We also thank the Drosophila Genomics Resource Center (supported by NIH grant 2P40OD010949) for cDNA clones. We thank Dr. Andrew Lin also for constructive comments on the manuscript. M.P. was supported by the Israel Science Foundation (ISF, 343/18) and the United States-Israel Binational Science Foundation (BSF, 2019026 and 2020636). T.H. was supported by NSF (2034783), BSF (2019026), and NIH (R01DC018874). A.M.D. was supported by NIH (F32MH125582).

AUTHOR CONTRIBUTIONS

Project initiation, M.P.; conceptualization, J.E.M. and M.P.; methodology, J.E.M., A.M.D., T.H., and M.P.; software, M.P.; formal analysis, J.E.M., T.H., and M.P.; investigation, J.E.M., A.M.D., T.H., and M.P.; writing - original draft, J.E.M., A.M.D., T.H., and M.P.; writing - review & editing, J.E.M., A.M.D., T.H., and M.P.; visualization, J.E.M. and M.P.; supervision, T.H. and M.P.; funding acquisition, T.H. and M.P.

DECLARATION OF INTERESTS

The authors declare no competing interests.

Received: May 22, 2022 Revised: August 15, 2022 Accepted: September 4, 2022 Published: September 20, 2022

REFERENCES

- 1. Watabe-Uchida, M., and Uchida, N. (2018). Multiple dopamine systems: weal and woe of dopamine. Cold Spring Harb. Symp. Quant. Biol. 83,
- 2. Garris, P.A., Ciolkowski, E.L., Pastore, P., and Wightman, R.M. (1994). Efflux of dopamine from the synaptic cleft in the nucleus accumbens of the rat brain. J. Neurosci. 14, 6084-6093.
- 3. He, K., Huertas, M., Hong, S.Z., Tie, X.X., Hell, J.W., Shouval, H., and Kirkwood, A. (2015). Distinct eligibility traces for LTP and LTD in cortical synapses. Neuron 88, 528-538.
- 4. Yagishita, S., Hayashi-Takagi, A., Ellis-Davies, G.C.R., Urakubo, H., Ishii, S., and Kasai, H. (2014). A critical time window for dopamine actions on the structural plasticity of dendritic spines. Science 345, 1616-1620.
- 5. Hige, T., Aso, Y., Modi, M.N., Rubin, G.M., and Turner, G.C. (2015). Heterosynaptic plasticity underlies aversive olfactory learning in Drosophila. Neuron 88, 985-998.
- 6. Hromádka, T., DeWeese, M.R., and Zador, A.M. (2008). Sparse representation of sounds in the unanesthetized auditory cortex. PLoS Biol. 6, e16.
- 7. Jadhav, S.P., Wolfe, J., and Feldman, D.E. (2009). Sparse temporal coding of elementary tactile features during active whisker sensation. Nat. Neurosci. 12, 792-800.

- 8. Poo, C., and Isaacson, J.S. (2009). Odor representations in olfactory cortex: "sparse" coding, global inhibition, and oscillations. Neuron 62,
- 9. Stettler, D.D., and Axel, R. (2009). Representations of odor in the piriform cortex. Neuron 63, 854-864.
- 10. Vinje, W.E., and Gallant, J.L. (2000). Sparse coding and decorrelation in primary visual cortex during natural vision. Science 287, 1273-1276.
- 11. Olshausen, B.A., and Field, D.J. (2004). Sparse coding of sensory inputs. Curr. Opin. Neurobiol. 14, 481-487.
- 12. Field, D.J. (1994). What is the goal of sensory coding? Neural Comput. 6,
- 13. Kara, P., Reinagel, P., and Reid, R.C. (2000). Low response variability in simultaneously recorded retinal, thalamic, and cortical neurons. Neuron 27, 635-646.
- 14. Vogel, A., Hennig, R.M., and Ronacher, B. (2005). Increase of neuronal response variability at higher processing levels as revealed by simultaneous recordings. J. Neurophysiol. 93, 3548–3559.
- 15. Bale, M.R., and Petersen, R.S. (2009). Transformation in the neural code for whisker deflection direction along the lemniscal pathway. J. Neurophysiol. 102, 2771-2780.
- 16. Hige, T. (2018). What can tiny mushrooms in fruit flies tell us about learning and memory? Neurosci. Res. 129, 8-16.
- 17. Tanaka, N.K., Tanimoto, H., and Ito, K. (2008). Neuronal assemblies of the Drosophila mushroom body. J. Comp. Neurol. 508, 711-755.
- 18. Aso, Y., Hattori, D., Yu, Y., Johnston, R.M., Iyer, N.A., Ngo, T.-T.T.B., Dionne, H., Abbott, L.F., Axel, R., Tanimoto, H., et al. (2014). The neuronal architecture of the mushroom body provides a logic for associative learning. eLife 3, e04577.
- 19. Mao, Z., and Davis, R.L. (2009). Eight different types of dopaminergic neurons innervate the Drosophila mushroom body neuropil: anatomical and physiological heterogeneity. Front. Neural Circuits 3, 5.
- 20. Takemura, S.-Y., Aso, Y., Hige, T., Wong, A., Lu, Z., Xu, C.S., Rivlin, P.K., Hess, H., Zhao, T., Parag, T., et al. (2017). A connectome of a learning and memory center in the adult Drosophila brain. eLife 6, e26975.
- 21. Kim, Y.C., Lee, H.G., and Han, K.A. (2007). D1 dopamine receptor dDA1 is required in the mushroom body neurons for aversive and appetitive learning in Drosophila. J. Neurosci. 27, 7640-7647.
- 22. Qin, H., Cressy, M., Li, W., Coravos, J.S., Izzi, S.A., and Dubnau, J. (2012). Gamma neurons mediate dopaminergic input during aversive olfactory memory formation in Drosophila. Curr. Biol. 22, 608-614.
- 23. Han, P.L., Levin, L.R., Reed, R.R., and Davis, R.L. (1992). Preferential expression of the Drosophila rutabaga gene in mushroom bodies, neural centers for learning in insects. Neuron 9, 619-627.
- 24. Livingstone, M.S., Sziber, P.P., and Quinn, W.G. (1984). Loss of calcium/ calmodulin responsiveness in adenylate cyclase of rutabaga, a Drosophila learning mutant. Cell 37, 205-215.
- 25. Levin, L.R., Han, P.L., Hwang, P.M., Feinstein, P.G., Davis, R.L., and Reed, R.R. (1992). The Drosophila learning and memory gene rutabaga encodes a Ca2+calmodulin-responsive adenylyl cyclase. Cell 68, 479-489.
- 26. Busto, G.U., Cervantes-Sandoval, I., and Davis, R.L. (2010). Olfactory learning in Drosophila. Physiology 25, 338-346.
- 27. Tomchik, S.M., and Davis, R.L. (2009). Dynamics of learning-related cAMP signaling and stimulus integration in the Drosophila olfactory pathway. Neuron 64, 510-521.
- 28. Cohn, R., Morantte, I., and Ruta, V. (2015). Coordinated and compartmentalized neuromodulation shapes sensory processing in Drosophila. Cell 163, 1742–1755.
- 29. Handler, A., Graham, T.G.W., Cohn, R., Morantte, I., Siliciano, A.F., Zeng, J., Li, Y., and Ruta, V. (2019). Distinct dopamine receptor pathways underlie the temporal sensitivity of associative learning. Cell 178, 60-75.e19.
- 30. Berry, J.A., Phan, A., and Davis, R.L. (2018). Dopamine neurons mediate learning and forgetting through bidirectional modulation of a memory trace. Cell Rep. 25, 651-662.e5.



Current Biology Article

- Turner, G.C., Bazhenov, M., and Laurent, G. (2008). Olfactory representations by Drosophila mushroom body neurons. J. Neurophysiol. 99, 734–746.
- Honegger, K.S., Campbell, R.A.A., and Turner, G.C. (2011). Cellular-resolution population imaging reveals robust sparse coding in the Drosophila mushroom body. J. Neurosci. 31, 11772–11785.
- Lin, A.C., Bygrave, A.M., De Calignon, A., Lee, T., and Miesenböck, G. (2014). Sparse, decorrelated odor coding in the mushroom body enhances learned odor discrimination. Nat. Neurosci. 17, 559–568.
- Liu, X., and Davis, R.L. (2009). The GABAergic anterior paired lateral neuron suppresses and is suppressed by olfactory learning. Nat. Neurosci. 12. 53–59.
- 35. Campbell, R.A.A., Honegger, K.S., Qin, H., Li, W., Demir, E., and Turner, G.C. (2013). Imaging a population code for odor identity in the Drosophila mushroom body. J. Neurosci. 33, 10568–10581.
- Boto, T., Louis, T., Jindachomthong, K., Jalink, K., and Tomchik, S.M. (2014). Dopaminergic modulation of cAMP drives nonlinear plasticity across the Drosophila mushroom body lobes. Curr. Biol. 24, 822–831.
- Barnstedt, O., Owald, D., Felsenberg, J., Brain, R., Moszynski, J.P., Talbot, C.B., Perrat, P.N., and Waddell, S. (2016). Memory-relevant mushroom body output synapses are cholinergic. Neuron 89, 1237–1247.
- 38. Ren, G.R., Folke, J., Hauser, F., Li, S., and Grimmelikhuijzen, C.J.P. (2015). The A- and B-type muscarinic acetylcholine receptors from Drosophila melanogaster couple to different second messenger pathways. Biochem. Biophys. Res. Commun. 462, 358–364.
- Collin, C., Hauser, F., De Valdivia, E.G., Li, S., Reisenberger, J., Carlsen, E.M.M., Khan, Z., Hansen, N.O., Puhm, F., Søndergaard, L., et al. (2013). Two types of muscarinic acetylcholine receptors in Drosophila and other arthropods. Cell. Mol. Life Sci. 70, 3231–3242.
- Bielopolski, N., Amin, H., Apostolopoulou, A.A., Rozenfeld, E., Lerner, H., Huetteroth, W., Lin, A.C., and Parnas, M. (2019). Inhibitory muscarinic acetylcholine receptors enhance aversive olfactory learning in adult *Drosophila*. eLife 8, e48264.
- Scheffer, L.K., Xu, C.S., Januszewski, M., Lu, Z., Takemura, S.Y., Hayworth, K.J., Huang, G.B., Shinomiya, K., Maitlin-Shepard, J., Berg, S., et al. (2020). A connectome and analysis of the adult Drosophila central brain. eLife 9, 1–74.
- Cognigni, P., Felsenberg, J., and Waddell, S. (2018). Do the right thing: neural network mechanisms of memory formation, expression and update in Drosophila. Curr. Opin. Neurobiol. 49, 51–58.
- Croset, V., Treiber, C.D., and Waddell, S. (2018). Cellular diversity in the Drosophila midbrain revealed by single-cell transcriptomics. eLife 7, e34550
- Davie, K., Janssens, J., Koldere, D., De Waegeneer, M., Pech, U., Kreft, L., Aibar, S., Makhzami, S., Christiaens, V., Bravo González-Blas, C., et al. (2018). A single-cell transcriptome atlas of the aging Drosophila brain. Cell 174, 982–998.e20.
- 45. Venken, K.J.T., Schulze, K.L., Haelterman, N.A., Pan, H., He, Y., Evans-Holm, M., Carlson, J.W., Levis, R.W., Spradling, A.C., Hoskins, R.A., et al. (2011). MiMIC: a highly versatile transposon insertion resource for engineering Drosophila melanogaster genes. Nat. Methods 8, 737–743.
- Kondo, S., Takahashi, T., Yamagata, N., Imanishi, Y., Katow, H., Hiramatsu, S., Lynn, K., Abe, A., Kumaraswamy, A., and Tanimoto, H. (2020). Neurochemical organization of the Drosophila brain visualized by endogenously tagged neurotransmitter receptors. Cell Rep. 30, 284– 297.e5.
- Aso, Y., Ray, R.P., Long, X., Bushey, D., Cichewicz, K., Ngo, T.T., Sharp, B., Christoforou, C., Hu, A., Lemire, A.L., et al. (2019). Nitric oxide acts as a cotransmitter in a subset of dopaminergic neurons to diversify memory dynamics. eLife 8, e49257.
- Tully, T., and Quinn, W.G. (1985). Classical conditioning and retention in normal and mutant Drosophila melanogaster. J. Comp. Physiol. A 157, 263–277.

- McGuire, S.E., Mao, Z., and Davis, R.L. (2004). Spatiotemporal gene expression targeting with the TARGET and gene-switch systems in Drosophila. Sci. STKE 2004, pl6.
- Chen, T.W., Wardill, T.J., Sun, Y., Pulver, S.R., Renninger, S.L., Baohan, A., Schreiter, E.R., Kerr, R.A., Orger, M.B., Jayaraman, V., et al. (2013). Ultrasensitive fluorescent proteins for imaging neuronal activity. Nature 499, 295–300.
- Jing, M., Li, Y., Zeng, J., Huang, P., Skirzewski, M., Kljakic, O., Peng, W., Qian, T., Tan, K., Zou, J., et al. (2020). An optimized acetylcholine sensor for monitoring in vivo cholinergic activity. Nat. Methods 17, 1139–1146.
- 52. Hackley, C.R., Mazzoni, E.O., and Blau, J. (2018). cAMPr: a single-wave-length fluorescent sensor for cyclic AMP. Sci. Signal. 11, eaah3738.
- Sweeney, S.T., Broadie, K., Keane, J., Niemann, H., and O'Kane, C.J. (1995). Targeted expression of tetanus toxin light chain in Drosophila specifically eliminates synaptic transmission and causes behavioral defects. Neuron 14, 341–351.
- Baghdoyan, H.A., Lydic, R., and Fleegal, M.A. (1998). M2 muscarinic autoreceptors modulate acetylcholine release in the medial pontine reticular formation. J. Pharmacol. Exp. Ther. 286, 1446–1452.
- Douglas, C.L., Baghdoyan, H.A., and Lydic, R. (2001). M2 muscarinic autoreceptors modulate acetylcholine release in prefrontal cortex of C57BL/6J mouse. J. Pharmacol. Exp. Ther. 299, 960–966.
- Isaacman-Beck, J., Paik, K.C., Wienecke, C.F.R., Yang, H.H., Fisher, Y.E., Wang, I.E., Ishida, I.G., Maimon, G., Wilson, R.I., and Clandinin, T.R. (2020). SPARC enables genetic manipulation of precise proportions of cells. Nat. Neurosci. 23, 1168–1175.
- 57. Klapoetke, N.C., Murata, Y., Kim, S.S., Pulver, S.R., Birdsey-Benson, A., Cho, Y.K., Morimoto, T.K., Chuong, A.S., Carpenter, E.J., Tian, Z., et al. (2014). Independent optical excitation of distinct neural populations. Nat. Methods 11, 338–346.
- 58. Ferris, J., Ge, H., Liu, L., and Roman, G. (2006). G(o) signaling is required for Drosophila associative learning. Nat. Neurosci. 9, 1036–1040.
- Zhang, S., and Roman, G. (2013). Presynaptic inhibition of gamma lobe neurons is required for olfactory learning in Drosophila. Curr. Biol. 23, 2519–2527.
- Dubnau, J., Grady, L., Kitamoto, T., and Tully, T. (2001). Disruption of neurotransmission in Drosophila mushroom body blocks retrieval but not acquisition of memory. Nature 411, 476–480.
- McGuire, S.E., Le, P.T., and Davis, R.L. (2001). The role of Drosophila mushroom body signaling in olfactory memory. Science 293, 1330–1333.
- Krashes, M.J., Keene, A.C., Leung, B., Armstrong, J.D., and Waddell, S. (2007). Sequential use of mushroom body neuron subsets during Drosophila odor memory processing. Neuron 53, 103–115.
- 63. Pribbenow, C., Chen, Y.-C., Heim, M.-M., Laber, D., Reubold, S., Reynolds, E., Balles, I., Grimalt, R.S., Rauch, C., Rösner, J., et al. (2021). Postsynaptic plasticity of cholinergic synapses underlies the 5 induction and expression of appetitive memories in Drosophila. Preprint at bioRxiv. https://doi.org/10.1101/2021.07.01.450776.
- Liu, W.W., and Wilson, R.I. (2013). Glutamate is an inhibitory neurotransmitter in the Drosophila olfactory system. Proc. Natl. Acad. Sci. USA 110, 10294–10299.
- Thum, A.S., Knapek, S., Rister, J., Dierichs-Schmitt, E., Heisenberg, M., and Tanimoto, H. (2006). Differential potencies of effector genes in adult *Drosophila*. J. Comp. Neurol. 498, 194–203.
- Rohrbough, J., and Broadie, K. (2002). Electrophysiological analysis of synaptic transmission in central neurons of *Drosophila* larvae. J. Neurophysiol. 88, 847–860.
- Rozenfeld, E., Tauber, M., Ben-Chaim, Y., and Parnas, M. (2021). GPCR voltage dependence controls neuronal plasticity and behavior. Nat. Commun. 12, 1–11.
- Eltze, M., Ullrich, B., Mutschler, E., Moser, U., Bungardt, E., Friebe, T., Gubitz, C., Tacke, R., and Lambrecht, G. (1993). Characterization of muscarinic receptors mediating vasodilation in rat perfused kidney. Eur. J. Pharmacol. 238, 343–355.

Current Biology

Article



- 69. Akk, G., and Auerbach, A. (1999). Activation of muscle nicotinic acetylcholine receptor channels by nicotinic and muscarinic agonists. Br. J. Pharmacol. 128, 1467-1476.
- 70. Chabala, L.D., Gurney, A.M., and Lester, H.A. (1986). Dose-response of acetylcholine receptor channels opened by a flash-activated agonist in voltage-clamped rat myoballs. J. Physiol. 371, 407-433.
- 71. Taussig, R., Iñiguez-Lluhi, J.A., and Gilman, A.G. (1993). Inhibition of adenylyl cyclase by Giα. Science 261, 218-221.
- 72. Zamponi, G.W., and Currie, K.P.M. (2013). Regulation of CaV2 calcium channels by G protein coupled receptors. Biochim. Biophys. Acta Rev. Biomembr. 1828, 1629-1643.
- 73. Kano, H., Toyama, Y., Imai, S., Iwahashi, Y., Mase, Y., Yokogawa, M., Osawa, M., and Shimada, I. (2019). Structural mechanism underlying G protein family-specific regulation of G protein-gated inwardly rectifying potassium channel. Nat. Commun. 10, 1-13.
- 74. Zars, T., Fischer, M., Schulz, R., and Heisenberg, M. (2000). Localization of a short-term memory in *Drosophila*. Science 288, 672-675.
- 75. Masuda-Nakagawa, L.M., Ito, K., Awasaki, T., and O'Kane, C.J. (2014). A single GABAergic neuron mediates feedback of odor-evoked signals in the mushroom body of larval Drosophila. Front. Neural Circuits 8, 35.
- 76. Papadopoulou, M., Cassenaer, S., Nowotny, T., and Laurent, G. (2011). Normalization for sparse encoding of odors by a wide-field interneuron. Science 332, 721-725.

- 77. Ray, S., Aldworth, Z.N., and Stopfer, M.A. (2020). Feedback inhibition and its control in an insect olfactory circuit. eLife 9, e53281.
- 78. Amin, H., Apostolopoulou, A.A., Suárez-Grimalt, R., Vrontou, E., and Lin, A.C. (2020). Localized inhibition in the Drosophila mushroom body. eLife 9. e56954.
- 79. Schindelin, J., Arganda-Carreras, I., Frise, E., Kaynig, V., Longair, M., Pietzsch, T., Preibisch, S., Rueden, C., Saalfeld, S., Schmid, B., et al. (2012). Fiji: an open-source platform for biological-image analysis. Nat. Methods 9, 676-682.
- 80. Lerner, H., Rozenfeld, E., Rozenman, B., Huetteroth, W., and Parnas, M. (2020). Differential role for a defined lateral horn neuron subset in naïve odor valence in Drosophila. Sci. Rep. 10, 6147.
- 81. Thévenaz, P., Ruttimann, U.E., and Unser, M. (1998). A pyramid approach to subpixel registration based on intensity. IEEE Trans. Image Process. 7,
- 82. Wu, J.S., and Luo, L. (2006). A protocol for dissecting Drosophila melanogaster brains for live imaging or immunostaining. Nat. Protoc. 1, 2110-2115
- 83. Livak, K.J., and Schmittgen, T.D. (2001). Analysis of relative gene expression data using real-time quantitative PCR and the 2(-Delta Delta C(T)) method. Methods 25, 402-408.
- 84. Clements, J., Dolafi, T., Umayam, L., Neubarth, N.L., Berg, S., Scheffer, L.K., and Plaza, S.M. (2020). neuPrint: analysis tools for EM connectomics. Preprint at bioRxiv. https://doi.org/10.1101/2020.01.16.909465.





STAR***METHODS**

KEY RESOURCES TABLE

DEACENT OF DECOUDES	SOURCE	IDENTIFIED
REAGENT or RESOURCE	SOURCE	IDENTIFIER
Antibodies		
Rabbit polyclonal anti-HA tag antibody - ChIP Grade	Abcam	Cat# ab9110; RRID: AB_307019
Mouse anti-Bruchpilot Monoclonal antibody	DSHB	Cat# nc82; RRID: AB_2314866
Alexa Fluor 488 goat anti-rabbit Polyclonal antibody	Abcam	Cat# ab150077; RRID: AB_2630356
Alexa Fluor 647 goat anti-mouse Polyclonal antibody	Abcam	Cat# ab150115; RRID: AB_2687948
Chemicals, peptides, and recombinant proteins		
All-trans retinal	Sigma-Aldrich	Cat# R2500; CAS: 116-31-4
3-octanol	Sigma-Aldrich	Cat# W358126; CAS: 589-98-0
MCH (4-Methylcyclohexanol)	Sigma-Aldrich	Cat# 153095; CAS: 589-91-3
IPA (Isopentyl acetate)	Sigma-Aldrich	Cat# 306967; CAS: 123-92-2
Mineral oil	Sigma-Aldrich	Cat# 330779; CAS: 8042-47-5
Triton-X-100	Sigma-Aldrich	Cat# HFH10
Dopamine Hydrochloride	Alfa Aesar	Cat# A11136; CAS: 62-31-7
Acetylcholine	Sigma-Aldrich	Cat# A6625; CAS: 60-31-1
TTX (Tetrodotoxin citrate)	Alomone Labs	Cat# T-550; CAS: 18660-81-6
Experimental models: Organisms/strains		
D. melanogaster: w ¹¹¹⁸	BDSC	Cat# 5905; RRID: BDSC_5905
D. melanogaster: MB247-GAL4	BDSC	Cat# 50742; RRID: BDSC_50742
D. melanogaster: c305a-GAL4	BDSC	Cat# 30829; RRID: BDSC_30829
D. melanogaster: OK107-GAL4	BDSC	Cat# 854; RRID: BDSC_854
D. melanogaster: MB247-lexA-lexAop-GCaMP6f	A gift from Dr. Andrew Lin	N/A
D. melanogaster: UAS-mAChR-B RNAi 1	BDSC	Cat# 67775; RRID: BDSC_67775
D. melanogaster: UAS-mAChR-B RNAi 2	VDRC	Cat# 107137; RRID: FlyBase_FBst0472091
D. melanogaster: UAS-Dcr-2	BDSC	Cat# 24651; RRID: BDSC_24651
D. melanogaster: tub-GAL80ts	BDSC	Cat# 7108; RRID: BDSC_7108
D. melanogaster: TI{2A-GAL4}mAChR-B[2A-GAL4]	BDSC	Cat# 84650; RRID: BDSC_84650
D. melanogaster: SPARC2-I-CsChrimson::tdTomato	BDSC	Cat# 84144; RRID: BDSC_84144
D. melanogaster: MiMIC-mAChR-B-GAL4	Generated in-house, as previously described ⁴⁰	N/A
D. melanogaster: elav-GAL4	BDSC	Cat# 458; RRID: BDSC_458
D. melanogaster: nSyb-IVS-PhiC31	BDSC	Cat# 84151; RRID: BDSC_84151
D. melanogaster: GMR71G10-GAL4	BDSC	Cat# 39604; RRID: BDSC_39604
D. melanogaster: GMR28H05-GAL4	BDSC	Cat# 49472; RRID: BDSC_49472
D. melanogaster: UAS-TNT	BDSC	Cat#28838; RRID: BDSC_28838
D. melanogaster: UAS-GACh3.0	BDSC	Cat# 86549; RRID: BDSC_86549
D. melanogaster: UAS-cAMPr	A gift from Dr. Justin Blau	N/A
D. melanogaster: UAS-mCD8-GFP	BDSC	Cat# 32186; RRID: BDSC_32186
D. melanogaster: UAS-GCaMP6f (attP40)	BDSC	Cat#42747; RRID: BDSC_42747
D. melanogaster: UAS-GCaMP6f (VK00005)	BDSC	Cat#52869; RRID: BDSC_52869
D. melanogaster: UAS-mAChR-B	This Paper	N/A
D. melanogaster: UAS-mAChR-B-HA	This paper	N/A
Critical commercial assays		
VECTASHIELD PLUS Antifade Mounting Medium	Vector laboratories	Cat# H-1900
EZ-RNA II kit	Biological Industries	Cat# 20-410-100
High-Capacity cDNA Reverse Transcription Kit	Thermo Scientific	Cat# AB-4374966
with RNase Inhibitor		

Current Biology

Article



Continued		
REAGENT or RESOURCE	SOURCE	IDENTIFIER
Oligonucleotides		
Primer: β-Tubulin Forward: CCAAGGGTCATTACACAGAGG	FlyPrimerBank, Purchased from HyLabs	https://www.flyrnai.org/flyprimerbank; DRSC/TRiP Functional Genomics Resources and DRSC-BTRR; RRID: SCR_021963
Primer: β-Tubulin Reverse: ATCAGCAGGGTTCCCATACC	FlyPrimerBank, Purchased from HyLabs	https://www.flymai.org/flyprimerbank; DRSC/TRiP Functional Genomics Resources and DRSC-BTRR; RRID: SCR_021963
Primer: mAChR-B Forward: ATGCGGTCGCTTAACAAGTC	FlyPrimerBank, Purchased from HyLabs	https://www.flyrnai.org/flyprimerbank; DRSC/TRiP Functional Genomics Resources and DRSC-BTRR; RRID: SCR_021963
Primer: mAChR-B Reverse: GCTCCCTTCTAAGGCTCCAG	FlyPrimerBank, Purchased from HyLabs	https://www.flyrnai.org/flyprimerbank; DRSC/TRiP Functional Genomics Resources and DRSC-BTRR; RRID: SCR_021963
Recombinant DNA		
cDNA: GEO08261	Drosophila Genomics Resource Center	https://dgrc.bio.indiana.edu//stock/1654134; GEO08261; DGRC Stock# 1654134; RRID: DGRC_1654134
Plasmid: pBID-UASc	Addgene	http://www.addgene.org/35200/; Cat# 35200; RRID: Addgene_35200
Software and algorithms		
MATLAB	MathWorks	https://www.mathworks.com/products/ matlab.html; RRID: SCR_001622
GraphPad Prism	GraphPad Software	https://www.graphpad.com/scientific-software/prism/; RRID: SCR_002798
StepOne Software	Applied Biosystems	http://downloads.thermofisher.com/Instrument_ Software/qPCR/Step-1/SOP23_Release%20 Notes_4482516.pdf; StepOne Software; RRID: SCR_014281
Fiji	Schindelin et al. ⁷⁹	https://fiji.sc/; RRID: SCR_002285
neuPrint	HHMI's Janelia Research Campus ⁶²	https://neuprint.janelia.org/?dataset=hemibrain: v1.2.1&qt=findneurons
Python (Spyder)	Spyder Doc Contributors, MIT License, Powered by Sphinx 3.5.4	https://www.spyder-ide.org/; RRID: SCR_017585
MScan	Sutter Instrument	https://www.sutter.com/MICROSCOPES/mcs.html
LabVIEW	National Instruments	https://www.ni.com/en-il/shop/labview.html; RRID: SCR_014325
LAS AF	Leica Microsystems	N/A

RESOURCE AVAILABILITY

Lead contact

Further information and requests for resources and reagents should be directed to and will be fulfilled by the lead contact, Moshe Parnas (mparnas@tauex.tau.ac.il).

Materials availability

Flies generated for this paper, data and code used to generate the figures will be available upon request. Requests should be directed to and will be fulfilled by the lead contact, Moshe Parnas (mparnas@tauex.tau.ac.il).

Data and code availability

The data and code used to generate Figures 1, 2, 3, 4, 5, 6, 7, and S1-S7 and Table S1, are available from the corresponding author upon request. The study did not generate any new code or dataset. Any additional information required to reanalyze the data reported in the paper is available from the lead contact upon request.





EXPERIMENTAL MODEL AND SUBJECT DETAILS

Fly strains

Fly strains were raised on cornmeal agar under a 12 h light/12 h dark cycle and studied 7–10 days post-eclosion. Strains were cultivated at 25°C. In cases where a temperature-sensitive gene product (GAL80^{ts}) was used, the experimental animals and all relevant controls were grown at 23°C. To allow expression of RNAi with GAL80^{ts}, experimental and control animals were incubated at 31°C for 7 days. Subsequent behavioral experiments were performed at 25°C.

Experimental animals carried transgenes over Canton-S chromosomes where possible to minimize genetic differences between strains. The following transgenes were used: UAS-GCaMP6f (BDSC #42747), MB247-lexA-lexAop-GCaMP6f (a gift from Dr. Andrew Lin), UAS-mAChR-B RNAi 1 (TRIP. HMS05691, Bloomington BDSC #67775), UAS-mAChR-B RNAi 2 (VDRC ID #107137), UAS-Dcr-2 (Bloomington BDSC #24651), tub-GAL80ts (BDSC #7108), MB247-GAL4 (BDSC #50742), OK107-GAL4 (BDSC #854), c305a-GAL4 (BDSC #30829), TI{2A-GAL4}mAChR-B[2A-GAL4] (BDSC #84650), MiMIC-mAChR-B-GAL4 (generated in-house, as previously described⁴⁰), elav-GAL4 (BDSC #458), UAS-TNT (BDSC #28838), nSyb-IVS-PhiC31 (BDSC #84151), TI{20XUAS-SPARC2-I-Syn21-CsChrimson::tdTomato-3.1}CR-P40 (BDSC #84144), GMR71G10-GAL4 (BDSC #39604), GMR28H05-GAL4 (BDSC #49472), UAS-GACh3.0 (BDSC #86549), UAS-cAMPr (a gift from Dr. Justin Blau), UAS-mCD8-GFP (BDSC #32186). UASmAChR-B and UAS-mAChR-B-HA were made in-house. Briefly, Drosophila mAChR-B was subcloned from a Drosophila Genomics Resource Center clone (DGRC, GEO08261) into the pBID-UASc plasmid using standard methods (Epoch Life Sciences). Transgenic strains were established by injecting pBID-UASc-mAChR-B constructs into attP40 landing site (BestGene).

METHOD DETAILS

Behavioral analysis

For behavior experiments, custom-built, fully automated apparatus were used. Single flies were placed in clear polycarbonate chambers (length 50 mm, width 5 mm, height 1.3 mm) with printed circuit boards (PCBs) at both floors and ceilings. Solid-state relays (Panasonic AQV253) connected the PCBs to a 50 V source.

Mass flow controllers (CMOSens PerformanceLine, Sensirion) were used to control the airflow. An odor stream (0.3 l/min) was obtained by circulating the airflow through vials filled with a liquid odorant and was combined to a carrier flow (2.7 l/min) yielding a 10 fold dilution from the odor source. The odor source was prepared at 10 fold dilution in mineral oil. Together, a final 100 fold dilution of odors was used. Fresh odors were prepared daily. Two identical odor delivery systems delivered odors independently to each half of the chamber. The 3 l/min total flow, consisting of the carrier flow and the odor stimulus flow, was split between 20 chambers. Thus, each half chamber received a flow rate of 0.15 l/min per half chamber. The airflow from the two halves of the chamber converged at a central choice zone.

The 20 chambers were stacked in two columns of 10 chambers. The chambers were backlit by 940 nm LEDs (Vishay TSAL6400). Images were obtained by a MAKO CMOS camera (Allied Vision Technologies) equipped with a Computar M0814-MP2 lens. The apparatus was operated in a temperature-controlled incubator (Panasonic MIR-154) maintained at 25°C.

A virtual instrument written in LabVIEW 7.1 (National Instruments) extracted fly position data from video images and controlled the delivery of odors and electric shocks. Data were analyzed in MATLAB 2017b (The MathWorks) and Prism 9 (GraphPad).

A fly's odor preference was calculated as the percentage of time that it spent on one side of the chamber. Three behavior protocols were used in this study as previously described. 40,67,80 (i) For conditioning experiments, OCT (or OCT:MCH mixture at the ratio of 60:40 or 20:80) and MCH were presented for two minutes from each side of the chamber to test the flies' relative preference. This was followed by a single training session of one minute (see below). Following the training session, flies were allowed to recover for 15 minutes and then they were tested again for preference between OCT and MCH (Figure 2). During training, MCH or OCT were paired with 12 equally spaced 1.25 s electric shocks at 50 V (CS⁺). The learning index was calculated as (preference for CS⁺ before training) – (preference for CS⁺ after training). (ii) For odor avoidance test, an odor was delivered to one side of the chamber and mineral oil to the other side for two minutes, and then the sides were switched (Figure S2C). The avoidance index was calculated as (preference for left side when it contains air) - (preference for left side when it contains odor). (iii) For nonspecific learning, flies were conditioned against MCH for one minute. This was followed by three minutes of recovery, and the valence of either OCT or MCH was evaluated as in point (ii) (Figure 7). The valence index was calculated as (preference for left side when it contains air) – (preference for left side when it contains odor). For all cases, flies were excluded from analysis if they entered the choice zone fewer than 4 times during odor presentation.

Functional imaging

Brains were imaged by two-photon laser-scanning microscopy (DF-Scope installed on an Olympus BX51WI microscope, Sutter). Flies were anesthetized on ice then a single fly was moved to a custom built chamber and fixed to aluminum foil using wax. The cuticle and trachea were removed in a window overlying the required area. The exposed brain was perfused with carbogenated solution (95% O₂, 5% CO₂) containing 103 mM NaCl, 3 mM KCl, 5 mM trehalose, 10 mM glucose, 26 mM NaHCO₃, 1 mM NaH₂PO₄, 3 mM CaCl₂, 4 mM MgCl₂, 5 mM N-Tris (TES), pH 7.3. Odors at 10⁻¹ dilution were delivered by switching mass-flow controlled carrier

Current Biology

Article



at 0.4 l/min and stimulus streams at 0.4 l/min (Sensirion) via software controlled solenoid valves (The Lee Company). This resulted in a final concentration of 5x10⁻² of odor delivered to the fly. Air-streamed odor was delivered through a 1/16 inch ultra-chemical-resistant Versilon PVC tubing (Saint-Gobain, NJ, USA) that was placed 5 mm from the fly's antenna.

Fluorescence was excited by a Ti-Sapphire laser (Mai Tai HP DS, 100 fs pulses) centered at 910 nm, attenuated by a Pockels cell (Conoptics) and coupled to a galvo-resonant scanner. Excitation light was focused by a 20X, 1.0 NA objective (Olympus XLUMPLFLN20XW), and emitted photons were detected by GaAsP photomultiplier tubes (Hamamatsu Photonics, H10770PA-40SEL), whose currents were amplified (Hamamatsu HC-130-INV) and transferred to the imaging computer (MScan 2.3.01). All imaging experiments were acquired at 30 Hz. When necessary, movies were motion-corrected using the TurboReg⁸¹ ImageJ plugin.⁷⁹ Δ F/F was calculated as was previously described. ³³ When a pharmacological effect was tested in the same fly, all ROIs Δ F/F values were calculated with the baseline fluorescence of the ROI prior to pharmacology. We excluded non-responsive flies and flies whose motion could not be corrected.

For all functional imaging experiments, a z axis stack was performed at the end of the experiment. The z-axis stack was used to identify the different lobes. In Figure 7, z-projections were used to identify planes and regions of interest in which there is expression of GCaMP but not CsChrimson.

Odors used

3-octanol (3-OCT), 4-methylcyclohexanol (MCH), and Isopentyl acetate (IPA) were purchased from Sigma-Aldrich (Rehovot, Israel) and were at the purest level available.

Optogenetic activation

For activation of CsChrimson, flies were collected 3 days post eclosion and grown for another 3-4 days on 1 mM all-trans retinal (R2500; Sigma-Aldrich) supplemented food in complete darkness before experimental testing was performed. For optogenetic experiments, brains were illuminated with 625 nm red light (GCS-0625-03; MIGHTEX LED) at 33 Hz (paired with a 5-s odor presentation).

Pharmacological application

The following drugs were used: Dopamine Hydrochloride (Alfa Aesar #A11136), ACh (Sigma-Aldrich #A6625) and TTX (Alomone Labs #T-550). In all cases stock solutions were prepared and diluted in external solution to the final concentration before experiments. For local application, a glass pipette filled was placed in close proximity to the MB lobe and was emptied using a pico injector (Harvard Apparatus, PLI-100).

Structural imaging

Brain dissections, fixation, and immunostaining were performed as described.⁸² To visualize native GFP fluorescence, dissected brains were fixed in 4% (w/v) paraformaldehyde in PBS (1.86 mM NaH₂PO₄, 8.41 mM Na₂HPO₄, 175 mM NaCl) and fixed for 20 minutes at room temperature. Samples were washed for 3×20 minutes in PBS containing 0.3% (v/v) Triton-X-100 (PBS-T). Primary antisera were rabbit polyclonal anti-HA (1:500, ab9110, Abcam), and mouse monoclonal anti-Bruchpilot - nc82 (1:50, DSHB). Secondary antisera were Alexa488 coupled to goat anti-rabbit or Alexa647 coupled to goat anti-mouse (1:250, all Abcam). Primary antisera were applied for 2 days and secondary antisera for 1 day in PBS-T at 4°C, followed by embedding in VECTASHIELD PLUS Antifade Mounting Medium (H-1900, Vector laboratories). Images were collected on a Leica TCS SP5 or SP8 confocal microscope and processed in ImageJ.

RNA purification, cDNA synthesis, and quantitative real-time PCR analysis

Total RNA from 60 adult heads was extracted using the EZ-RNA II kit (#20-410-100, Biological Industries, Kibbutz Beit-Haemek, Israel) for each biological replicate. Reverse transcription of total RNA (1000ng) into complementary DNA (cDNA) was performed using High-Capacity cDNA Reverse Transcription Kit with RNase Inhibitor (AB-4374966, Thermo Scientific, Massachusetts, USA). RT-PCR reactions were performed using Fast SYBR Green Master Mix (AB-4385612, Applied Biosystems, CA, USA) in a StepOnePlus instrument (Applied Biosystems, CA, USA). Primers (β-Tubulin, forward primer, CCAAGGGTCATTACACAGAGG, reverse primer, ATCAGCAGGGTTCCCATACC; mAChR-B, forward primer, ATGCGGTCGCTTAACAAGTC, reverse primer, GCTCCCTTCTAAGGCT CCAG) were calibrated, and a negative control was performed for each primer. Samples were measured in technical triplicates, and values were normalized according to mRNA levels of the β-Tubulin housekeeping gene. The amplification cycles were 95°C for 30s, 60°C for 15s, and 72°C for 10s. At the end of the assay, a melting curve was constructed to evaluate the specificity of the reaction. The fold change for each target was subsequently calculated by comparing it to the normalized value of the ELAV-gal4 parent. Quantification was assessed at the logarithmic phase of the PCR reaction using the 2- $\Delta\Delta$ CT method, as described previously.

Connectome data analysis

For the connectome analysis, the Hemibrain v1.2.1 dataset made publicly available by Janelia Research Campus^{41,84} was used. Hemibrain data was accessed via the Neuprint python package (https://github.com/connectome-neuprint/neuprint-python). To





distinguish between axo-axonal connections and dendro-dendritic connections, the connections were filtered based on the ROI in which they occur (i.e. Calyx for dendrites or α/β , α'/β' or γ' lobe).

QUANTIFICATION AND STATISTICAL ANALYSIS

Statistics

Statistical analyses were carried out in GraphPad Prism as described in Figure legends and Table S1.